



# Sedimentary structure of inferred cyclic-step bedforms in submarine volcanoclastic slope deposits, Cuatro Calas, south-east Spain

JAN H. VAN DEN BERG\*  and JÖRG LANG† 

\*Faculty of Geosciences, Utrecht University, Princetonlaan 8a, Utrecht, 3584 CB, The Netherlands (E-mail: j.h.vandenberg@uu.nl)

†Institut für Geologie, Leibniz Universität Hannover, Callinstraße 30, Hannover, 30167, Germany

Associate Editor – Matthieu Cartigny

## ABSTRACT

Cyclic steps are widespread on submarine slopes of many modern insular volcanoes. This paper provides the first detailed description and interpretation of the sedimentary structures and depositional architecture of cyclic-step deposits of such bedforms formed on the submarine slope of an ancient volcano. The partially depositional cyclic steps are preserved in a 67 m thick coset of 1 to 12 m thick cobble-based units of middle Miocene submarine volcanoclastics, exposed along a cliff outcrop in south-east Spain. The main structure in the units is unidirectional crude low-angle cross-bedding passing upward to centimetre to decimetre-scale diffuse stratification more or less parallel to the unit bounding surfaces. The depositional architecture produced by inferred sinuous to straight-crested cyclic steps is compared with deposits of crescent-shaped cyclic steps formed in confined settings. With a novel method, a maximum cyclic step height and length of 22 m and 460 m, respectively, have been calculated. The architecture of some of the thicker cyclic-step units is complicated by structures that were formed as cyclic-step trough-fills, by superimposed cyclic steps or downstream migrating antidunes. These structures possibly reflect adaptation processes of the bedform morphology to a lower strength of the hydraulic jumps and related density flows. In the upper, less well-exposed part of the succession more steeply inclined gravel backsets that probably represent deposits of crescent-shaped cyclic steps accreted in a more energetic, confined setting proximal to the coastal source of the density flows. A facies model of straight-crested cyclic steps is presented that may aid in the identification of similar bedforms in submarine volcanoclastic environments and comparable non-volcanic settings.

**Keywords** Backsets, cyclic steps, high-density turbidity current, submarine volcanoclastics, supercritical flow.

## INTRODUCTION

Detailed bathymetric studies during the past decade have revealed the presence of large cyclic steps with lengths in the order of 50 to 1000 m magnitude in modern submarine environments. Their depositional signatures have been described from seismic images (for an

overview see Slootman & Cartigny, 2020). So far, well-documented outcrop evidence of submarine cyclic steps is rare. It is restricted to some successions deposited in delta-front settings, submarine canyons and deep-water turbidite channel-lobe complexes (Ponce & Carmona, 2011; Postma *et al.*, 2014, 2016, 2021; Ventra *et al.*, 2015; Bain & Hubbard, 2016; Lang *et al.*,

2017; Ono & Plink-Björklund, 2018; Postma & Kleverlaan, 2018; Slootman *et al.*, 2019; Ghienne *et al.*, 2020).

Submarine slopes of volcanoes subject to dominant explosive activity are repeatedly affected by sediment density flows that create upper flow regime bedforms (Clare *et al.*, 2018). Extensive fields of large sediment waves have been found on the submarine slopes around almost all volcanic islands that were investigated by high-resolution bathymetric and seismic surveys (Casalbore *et al.*, 2010, Casalbore *et al.*, 2014, 2015, Casalbore *et al.*, 2021; Symons *et al.*, 2016; Clare *et al.*, 2018; Pope *et al.*, 2018; Santos *et al.*, 2019). These bedforms have either been inferred to be associated with a system of listric faults paralleling the depth contours, or as being formed by high-density flows (Pope *et al.*, 2018). The bedforms generally show the step-like cross-section and a gradual downslope change in geometry that characterize cyclic steps (Pope *et al.*, 2018; Casalbore *et al.*, 2021). Yet, to date, these large bedforms have not been identified in outcrops of submarine volcanoclastics. Their sedimentary structures are only known to some extent from high-resolution seismic profiles of modern submarine examples (Pope *et al.*, 2018). However, these profiles do not penetrate deeply

into the sediment and do not reveal the sedimentary architecture in detail. Large-scale cross-stratification in deposits of subaqueous volcanoclastic flows that might have originated from cyclic steps has been reported in only a few studies (Heinrichs, 1984; White, 1996; Allen *et al.*, 2007). The study of White (1996) describes up to about 1 m thick sigmoidal low-angle cross-bedded sets in the sedimentary deposits of a volcano in the Late Pleistocene Lake Bonneville, Utah, USA. The reason for being unnoticed is simply explained by the recent discovery of the submarine existence of cyclic-step bedforms, but also, as noted by Postma *et al.* (2014), Massari (2017) and Ono *et al.* (2021), because the large dimensions commonly attained by these bedforms makes their recognition difficult, especially in outcrops of limited size.

For non-volcanic submarine slopes the structure of cyclic-step deposits is described and explained by Postma *et al.* (2014) and Postma & Cartigny (2014), which provides the conceptual basis for the analysis in this paper. For convenience their top-cut-out Bouma model is summarized here with minor modifications of their illustration of the model (Fig. 1). The most important amendment of these is the addition of

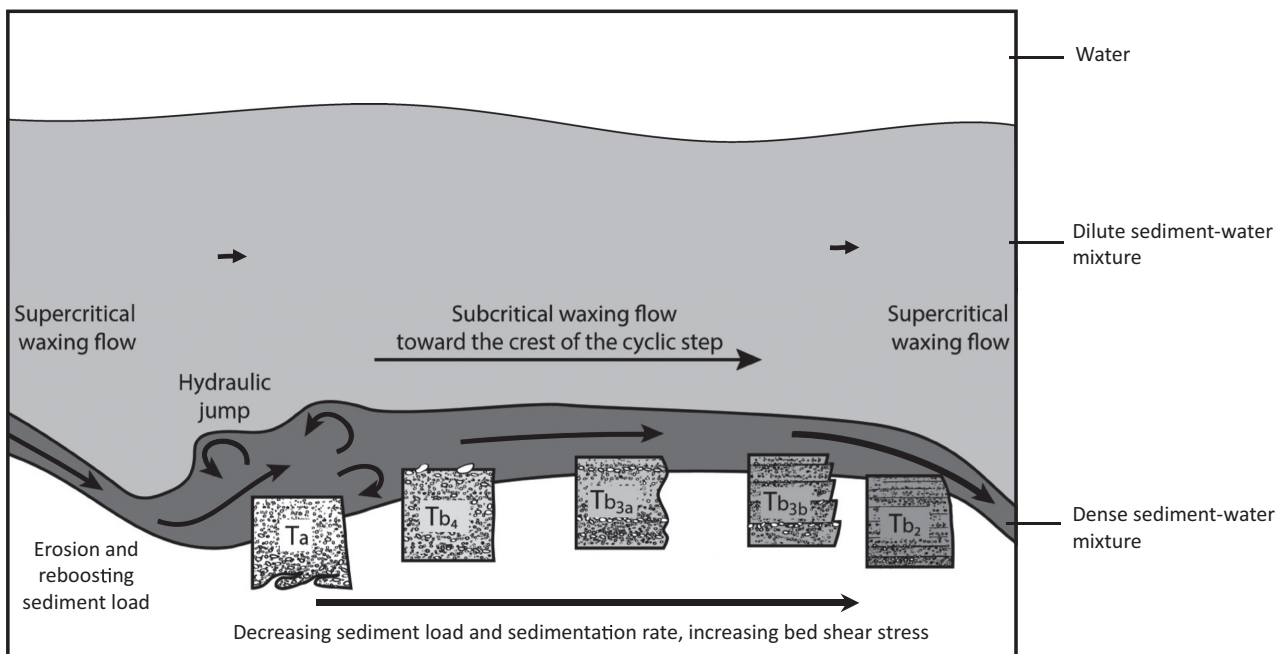


**Fig. 1.** Facies produced by deposition on submarine cyclic step. Flow along the lee-side of the bedform is supercritical and erosive while flow along the stoss side is subcritical and depositional (modified after Postma & Cartigny, 2014).

their assumption of a second flow interface. This is important because the morphology of a field of cyclic steps of more or less equal size and shape often found in nature can only persist by the presence of a well-defined near-bed dense underflow with a constant thickness averaged over a series of successive cyclic steps (Van den Berg *et al.*, 2017). Accordingly, approximately the same volume of sand transferred from the dense basal layer to the more dilute upper density flow has to settle back down along the cyclic step's stoss-side. Conversely, a one-layer density flow dilutes and thickens quickly by mixing with the overlying ambient fluid (e.g. Mastbergen & Berg, 2003), resulting in a downstream increase length of cyclic steps. The existence of a dense near-bed flow layer over cyclic steps was observed in flume experiments (Cartigny *et al.*, 2013) and in nature (Hughes Clarke, 2016; Paull *et al.*, 2018).

In the Postma & Cartigny (2014) model two main facies are distinguished that comprise cyclic-step deposits and correspond to the lower two divisions of the classical Bouma sequence: deposits that are generated under the influence of the internal hydraulic jump ( $Ta$ ; see also Postma *et al.*, 2009) and those that represent the waxing of the subcritical flow on the stoss-side of the cyclic-step bedform ( $Tb$ ). The hydraulic jump zone is represented by deposits devoid of primary sedimentary structures from very rapid accumulation under virtually no horizontal shear, with flame structures, convolutions and rip-up clasts that are produced by strong lift forces at the base of the internal hydraulic jump. The stoss-side deposits originate from rapid deposition by concentrated sediment dispersions (traction carpets), as defined and explained by Dzulynski & Sanders (1962) and Sohn (1997). These thin, basal sediment layers are dragged along by the overriding density flow. In a downflow direction along the cyclic step's stoss side they deposit varying sedimentary structures reflecting an increase in flow strength and decreasing sedimentation rate. As shown in Fig. 1, in downflow successions the following facies are accumulated on the bedform stoss-side: virtually structureless deposits ( $Tb_4$ ) produced by a combination of a very high sedimentation rates and a low flow strength; low angle crude stratification ( $Tb_{3a}$ ), which lacks sharp or erosional boundaries, due to high rates of aggradation; variable centimetre-thick spaced stratification ( $Tb_{3b}$ ), representing unsteady but continuous sedimentation and eventually planar

lamination with a spacing less than 0.5 cm and internal erosion planes reflecting a further increase in flow strength and decrease in net sedimentation rate ( $Tb_2$ ). The low-angle inclination decreases from the base of the crude bedding upward.

The aims of the paper are: (i) to describe and interpret the sedimentary structures and depositional architectures of submarine cyclic-step units preserved in a 67 m thick coset of volcanoclastic deposits; and (ii) to compare the inferred bedforms with cyclic-step features on modern submarine volcanic slopes. The studied case is a superb 400 m long continuous outcrop of Miocene volcanoclastics exposed at the seaward face of the protruding hill between the pocket beaches of the Cala Cerrada (also known as Cala de los Cocedores) and the Cala de la Carolina. These two small bays belong to a group of four that together bear the name Cuatro Calas, situated at the border of the provinces of Almería and Murcia, south-east Spain (Fig. 2B). The cliff site is still accessible on foot from the Cala Cerrada by the abrasion platform at spring low tide and low wave conditions.

The data for this study were obtained by geological field measurements and by taking photographs from the marine abrasion platform and from sea using a dinghy. A new method is developed to estimate cyclic-step bedform height and length from the preserved deposits. The obtained dimensions are compared with observations from modern submarine volcanoclastic cyclic steps. These results provide broadly applicable criteria for recognizing the sedimentary structures of partly depositional cyclic steps in submarine volcanoclastic successions and comparable submarine settings and linking them to cyclic-step bedforms observed in modern environments.

## STUDY AREA AND GEOLOGICAL SETTING

The regional geodynamics of the study area is governed by a major left lateral transcurrent zone, known as the Eastern Betics Shear Zone (Fig. 2A; Alfaro *et al.*, 2002). This zone is generated in response to continental indentation alongside the south-east margin of Iberia, related to the northward shift of the north-west African continental plate. This process triggered the development of the Águilas Arc (Coppier *et al.*, 1989) from the middle Miocene until the Quaternary (Silva *et al.*, 1993) and possibly also

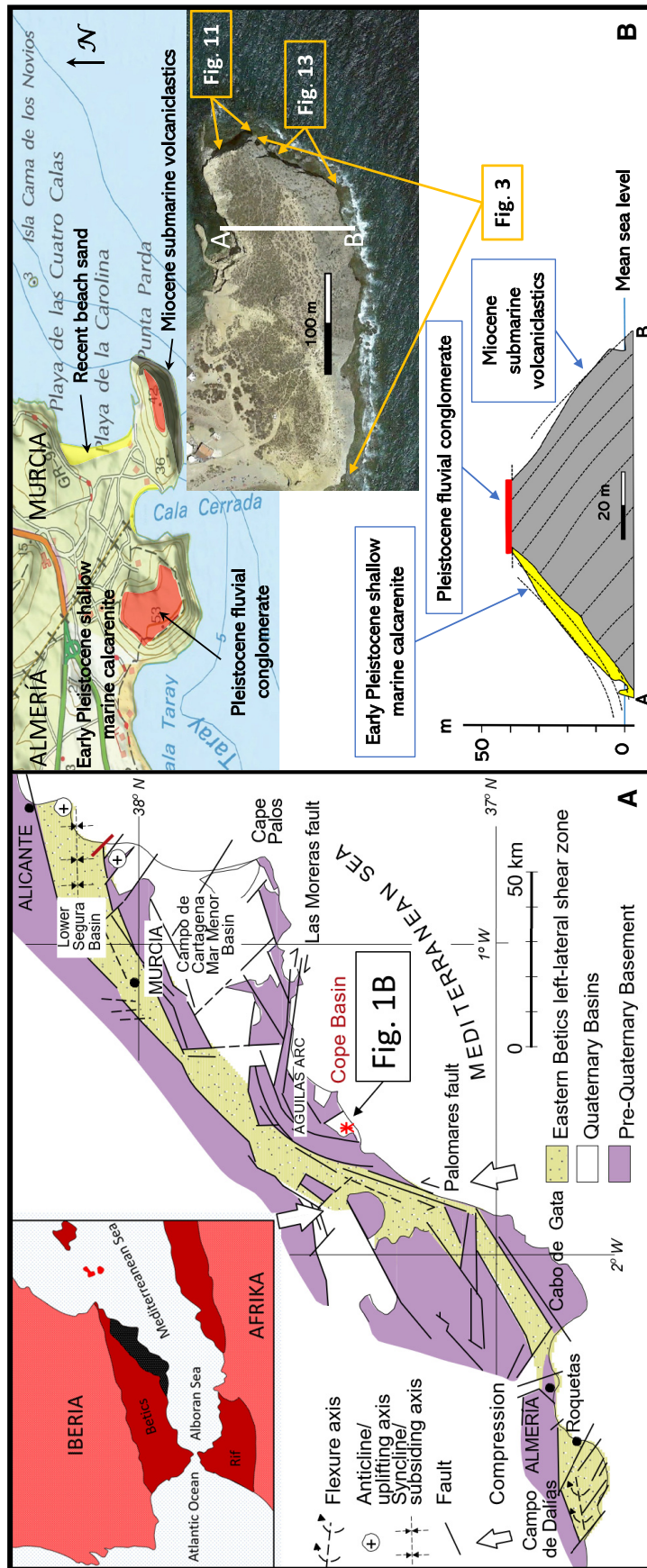


Fig. 2. Location of study area within the Cope Basin and tectonic framework of eastern Betic Cordillera. (A) Geological map and cross-section. (B) Geological and tectonic sketch (after Zazo *et al.*, 2012). Inset shows the extent of the study area, highlighted in black. Dashed lines in cross-section represent tectonic dip. Satellite image showing location of geological cross-section and camera location at sea of photographs displayed in some figures.

initiated the volcanic activity as the volcanoclastics in the cliff outcrop comprised in the succession discussed here are dated at 14.1 Ma (Bellon *et al.*, 1983). The Águilas Arc is delimited to the south-west and north-east by systems of left-lateral and right-lateral strike-slip faults (Palomares and Moreras fault systems, see Fig. 2A).

The volcanoclastic deposits are classified as calc-alkaline andesites (Aparicio, 2015). Petrographically similar volcanic rocks are also exposed in four nearby spots along the coast (Arana-Castillo, 2007). The cliff outcrop is situated in the Cope Basin, a small detachment structure within the Águilas Arc (Dabrio *et al.*, 1991; Bardají, 1999; Zazo *et al.*, 2013). Early Pleistocene subsidence of this basin led to the formation of a shallow bay (Dabrio *et al.*, 1991), where fossiliferous calcarenites were deposited. After the area became subaerial due to a general fall of sea level, gravelly sands were deposited by alluvial fans and deltas (Zazo *et al.*, 2013). These deposits represent cold periods of the Middle Pleistocene that correlate with global glacial phases (Harvey, 2002). They form well-cemented conglomerate caps on the hills of the Cuatro Calas area. The grey Miocene volcanoclastic succession is exposed below the soft, yellow, fossiliferous marine calcarenite strata and fluvial conglomerates (Fig. 2B). Instead of being separated from the calcarenites by a fault, as suggested by Dabrio *et al.*, 1991), the Early Pleistocene marine deposits overlap a pre-existing relief representing the remnant topography of a volcanic edifice, locally with a basal conglomerate. The Miocene volcanoclastic layers in the cliff were affected by tectonic movements before and after the deposition of the calcarenites. The tectonic tilt is about 35° towards the south-east. Although the volcanoclastic deposits are submarine, as proved by foraminifera (Grievaud *et al.*, 1990), the roundness of the andesite pebbles and cobbles contradicts a submarine origin of these clasts: When tephra bombs are ejected from a vent directly into water, or indirectly through the air as ballistic debris, its instant cooling leads to quench fragmentation (Cas & Giordano, 2014), resulting in sharp-edged hyaloclasts. Thus, rounded pebbles and cobbles indicate initial deposition on the subaerial part of a volcano, before being transported downslope by sediment density flows. They may have accumulated first in beaches, where wave action contributed to their roundness before being entrained to deeper water by high density flows, as commonly inferred in

marine environments (Winsemann & Seyfried, 1991; Allen *et al.*, 2007; Lang *et al.*, 2017) and also suggested for the Cuatro Calas volcanoclastics (Aparicio, 2015). Clare *et al.* (2018) mention a wide variety of mechanisms by which sediment from oversupplied volcanic subaerial depositional environments can be incorporated into density flows and transported to deeper water. However, it is not known what triggering mechanisms dominate and how these can be deduced from the deposits. These questions lie beyond the aim of this study. The palaeo-depth of the sea around or nearby the volcano is also uncertain. In a recent palaeogeographic map of the western Alboran Sea by Do Couto *et al.* (2016), based on tectonic and stratigraphic information, the presence of the Cuatro Calas submarine volcanoclastics was obviously overlooked, because the map suggests that the area was subaerially exposed during the Langhian (14 to 15 Ma). The volcano therefore probably rose from a shallow-marine area and may have been an island or connected with the mainland.

## DESCRIPTION OF SEDIMENTARY STRUCTURES

The cliff exposure (Fig. 3) shows a coset of 1 to 12 m thick sedimentary units consisting almost entirely of volcanoclastic, coarse-grained sand and sub-rounded, dark, pebble to boulder-sized andesite clasts. All stratal units have a cobble-base (CB-units) and are numbered in the log of Fig. 4, except for some poorly exposed ones in the upper part of the outcrop. To facilitate comparison this numbering is consistently referred to throughout this paper. The CB-units generally contain one or more sigmoidal 1 to 4 m thick, low-angle structures that pass upward into up to 7 m thick packages of diffuse stratification that parallel the unit boundaries (Fig. 4). In the lower part of the outcrop sand is the dominant grain size, while in the upper part most of the CB-units are gravel-dominated. Sand-dominated CB-units always start with a 0.5 to 2.0 m thick pervasive, coarse-tail normal graded layer with cobbles at the base (Fig. 5). This graded layer shows crude, unidirectional low-angle bedding or is partly or completely devoid of any primary structures. In the latter case, faintly recognizable dish-shaped structures approximately 1 dm wide may be present (Fig. 6). In the lower part of the coset the graded division is always structureless (Figs 4 and 5, and Data S1). The cobble-

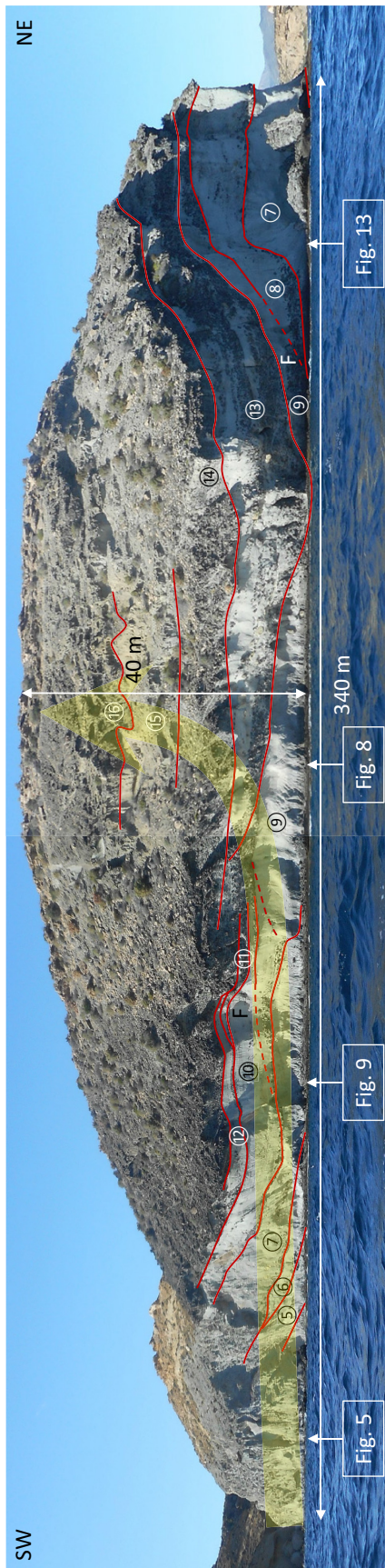


**Fig. 3.** Panoramic view of the studied coastal cliff from the south-east. Circled numbers identify specific cobble-based units (see also Fig. 4). Red lines outline bounding surfaces of cobble-based units. Dashed red lines indicate erosional discontinuities. 'F' letters indicate fill-structures. Yellow arrow denotes track of the sedimentary log presented in Fig. 4. See Fig. 2B satellite image for location.

base is locally underlain by a decimetre-thick, massive sand layer which forms the lower unit boundary ('M' in Fig. 7A).

The volcanoclastic succession shows a coarsening-upward trend, or, more precisely, a thickening upward trend for the graded cobble-layers at the base of individual units. In the higher parts of the succession, some 2 to 4 m thick units of crude cross-bedding are found consisting almost entirely of cobbles and pebbles (Figs 3, 4 and 8: CB-unit 11 and higher). Most of the western and middle part of the cliff show the sedimentary units in more or less cross-bed down-dip-oriented cross-sections. In these longitudinal views the erosional bases of the units, marked by the dark andesite pebbles and cobbles, show straight to slightly scooped profiles (Figs 3 and 9). At the coastal abrasion platform below the cliff the cobble bases are also straight zones that can easily be followed, some for tens of metres (Fig. 10). Despite the large size of the outcrop, the full lateral extent of most of the thicker CB-units cannot be determined. One of them – CB-unit 7 – can be traced in both the western and eastern part of the outcrop (Fig. 3), indicating a cross-bed down-dip length in excess of 300 m. A large transverse section is present in the easternmost part, showing CB-units with planar bounding surfaces (Fig. 11). In cross-bed dip-oriented sections the shape of the lower, sand-dominated units is tabular (Figs 3 and 9) and in the abrasion platform the cobble concentrations along the lower unit boundaries approximate straight lines (Fig. 10). From this it follows that the geometry of these CB-units is also tabular. Comparison of cross-bed inclinations along the outcrop indicates that all sigmoidal structures of the volcanoclastic succession have the same east to north-easterly directed low-angle cross-bed direction. There are no other reliable palaeoflow indicators. Imbrication was found only at a few locations, where it is weakly developed, possibly due to the subrounded nature of the clasts. The preferred orientation of the long axis of the clasts is either oblique with respect to the basal bounding surface of the CB-unit, suggesting a palaeoflow opposite to the cross-bed direction (Fig. 5), or almost perpendicular to it (Fig. 7A: indicated by 'V'). The uppermost CB-units of the succession are less well exposed. Their cross-bedding and bounding surfaces seem to be more trough-shaped. Observed deformation structures are restricted to one large flame structure at the base of one of the lowermost units (Fig. 4; Data

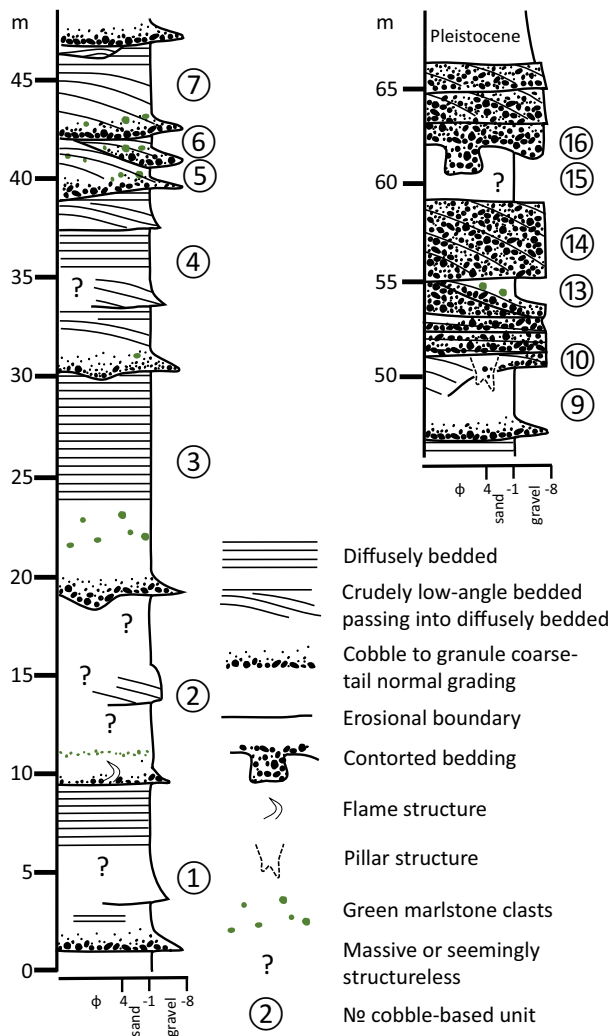


**Fig. 4.** Sedimentary log of the exposed volcaniclastics based on the western and middle part of the studied cliff following the track indicated by the yellow arrow in Fig. 3. Massive facies are defined based on the ascertained absence of primary sedimentary structures. Seemingly structureless facies are defined on the possible absence of visible sedimentary structures, possibly due to insufficient quality of exposure.

S1), an isolated sand–gravel pocket with pillar structures (Fig. 7B: indicated by ‘E’), two groups of dish structures (Fig. 6), and a contorted bed that involves CB-units 15 and 16 (Figs 3, 4 and 8).

In the middle of the outcrop a series of CB-units is exposed in an 80 m long cross-bed dip-oriented section (Fig. 9). Here, the ideal weathering conditions in correspondence with an overhanging cliff have resulted in an exposure of extraordinarily high quality, where faint structures otherwise non-discernible to the

naked eye can be well observed. The following description of the sedimentary architecture of the cobble-bounded units is mainly based on this section.

Two types of CB-units are distinguished, simple and complex. A simple CB-unit consists of a set of essentially conformable, sigmoidal, low-angle cross-strata. Layers of dark andesite cobbles at the base of each coarse sand dominated unit accentuate the erosional bounding surfaces. The basal, structureless or crudely bedded layer generally is accompanied by the pervasive coarse-tail normal grading, as mentioned above. Crude bedding is defined here as irregular, decimetre to metre-scale stratification with diffuse strata boundaries and some erosional discontinuities that disappear upward (Fig. 6). Some of the pebble and cobble concentrations form strings that follow the alignment of a scour at the base of CB-units in a westerly direction (Figs 6 and 9, indicated by ‘R’). The cobble layers are either devoid of sedimentary structures (massive), show a low-angle crude bedding, or, in other parts of the outcrop, appear structureless due to insufficient quality of exposure. Green marlstone clasts up to 0.5 to 1.0 m in diameter may be present at the upward transition from crude bedding to diffuse stratification and within the lower part of the latter stratification, (Figs 4, 5, 6, 8, 9 and 11). These clasts generally are matrix-supported, but may also form a clast-supported fabric at the transition between crude and diffuse bedding. In the latter case, evidence for erosional scour alongside the clasts indicates deposition shortly before settling of the surrounding coarse sand–granule matrix (Fig. 6, CB-unit 6). In an upward direction the low-angle crude bedding passes into more regular, less inclined diffuse stratification in medium-grained to very coarse-grained sand, with a few fine gravel stringers (see Figs 6 and 9). A diffusely stratified facies is defined here following Sohn (1997), as a deposit composed of centimetre to decimetre-scale stratification, lacking distinct erosional boundaries and showing alternating coarsening-upward and fining-upward intervals (Fig. 12).

Locally within the CB-units, one or more smaller, decimetre to metre-scale sets of low-angle, sigmoidal or lens-shaped cross-bedding intercalate within the diffuse strata or appear at the top of the CB-unit (Figs 4, 5, 6, 7 and 13). The crude-bedding at the base of these sets, that for convenience will be named secondary units,

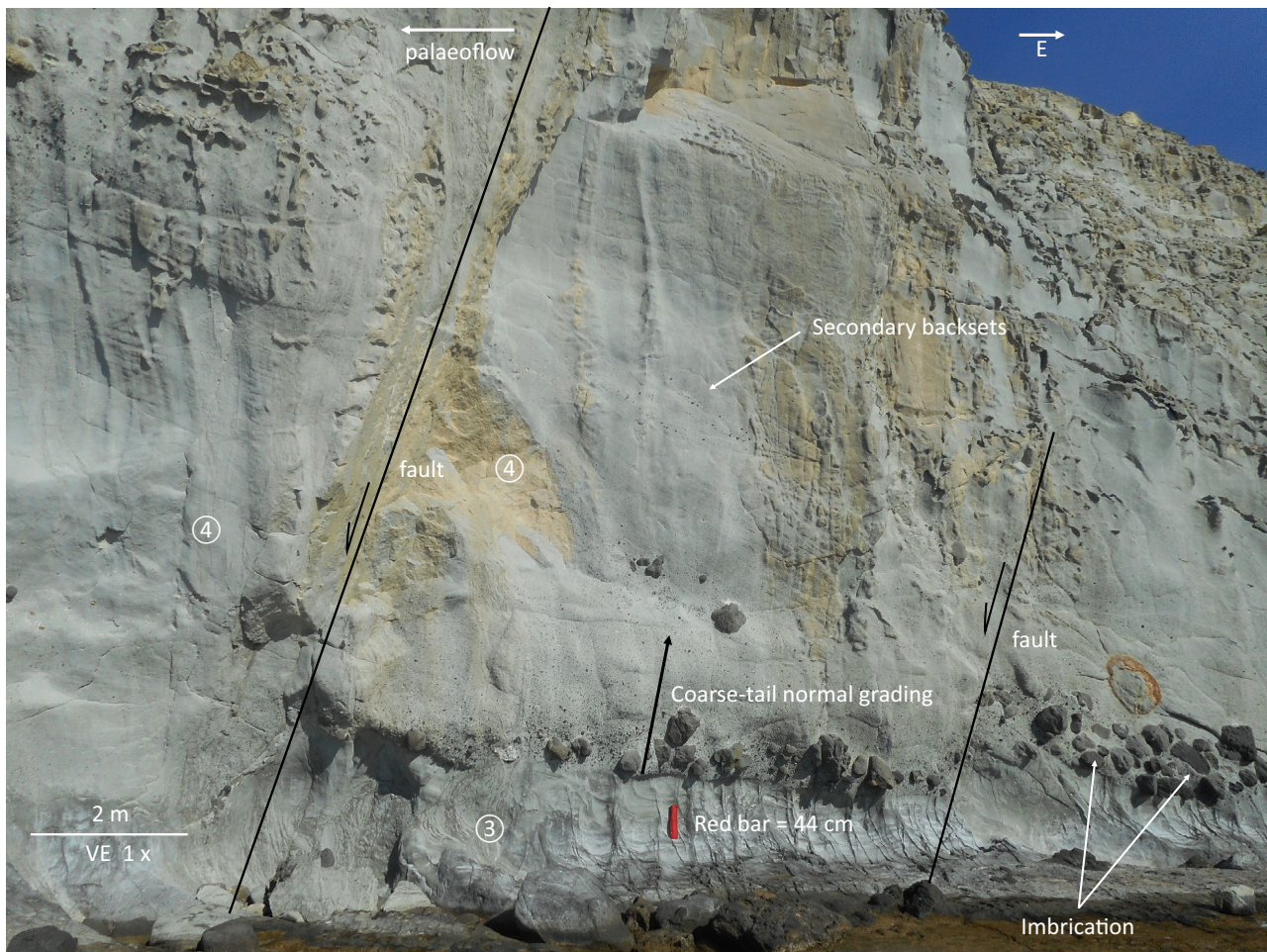


**Fig. 5.** Impression of faint, low-angle structures and cobble base of CB-unit 4, with characteristic coarse-tail normal grading and local andesite clast imbrication. Three closely spaced faults can be observed in the outcrop, two of which are shown here. The almost vertical normal faults show a 4 m, 1 m and 1.5 m displacement, respectively, cross the whole volcanoclastic succession as visible in the cliff, with an orientation of  $110^\circ$  (ESE) and hanging walls facing the SSW. See Fig. 3 for location.

do not have a cobble-base. They can be followed up to several tens of metres before disappearing, generally maintaining the same dip direction for cross-bed strata as the larger CB-units. Their internal structures, sometimes featuring oppositely directed low-angle cross-bedding are often not clearly exposed because of their faint nature and unfavourable weathering. The best examples are found in the middle part of the outcrop (Fig. 9), where two types of secondary units are found: (i) a large trough-fill structure that developed over the full thickness of the CB-unit; and (ii) smaller lens-shaped units. The first type is found in CB-unit 10. The sigmoidal cross-bedding of this secondary unit climbs along an erosional discontinuity

(Figs 7 and 9). Within the sigmoidal cross-bedding minor erosional discordances occur that bound wedges of less-inclined faint bedding (Fig. 7A: right part). Such wedges occasionally are also found at the base of CB-units (Fig. 7A: left part). Examples of the second type of secondary units can be observed at the top of the diffuse stratification in CB-units 6, 7 and 10 (Figs 6 and 7A: indicated by 'N'). They consist of diffusely stratified low angle cross-bedding with some erosional discontinuities. Most of their cross-bedding is oppositely directed to the main sigmoidal cross-bedding. The structures are hosted within a spoon-shaped scour, that may be the starting point of a convex-upward stratified lens.



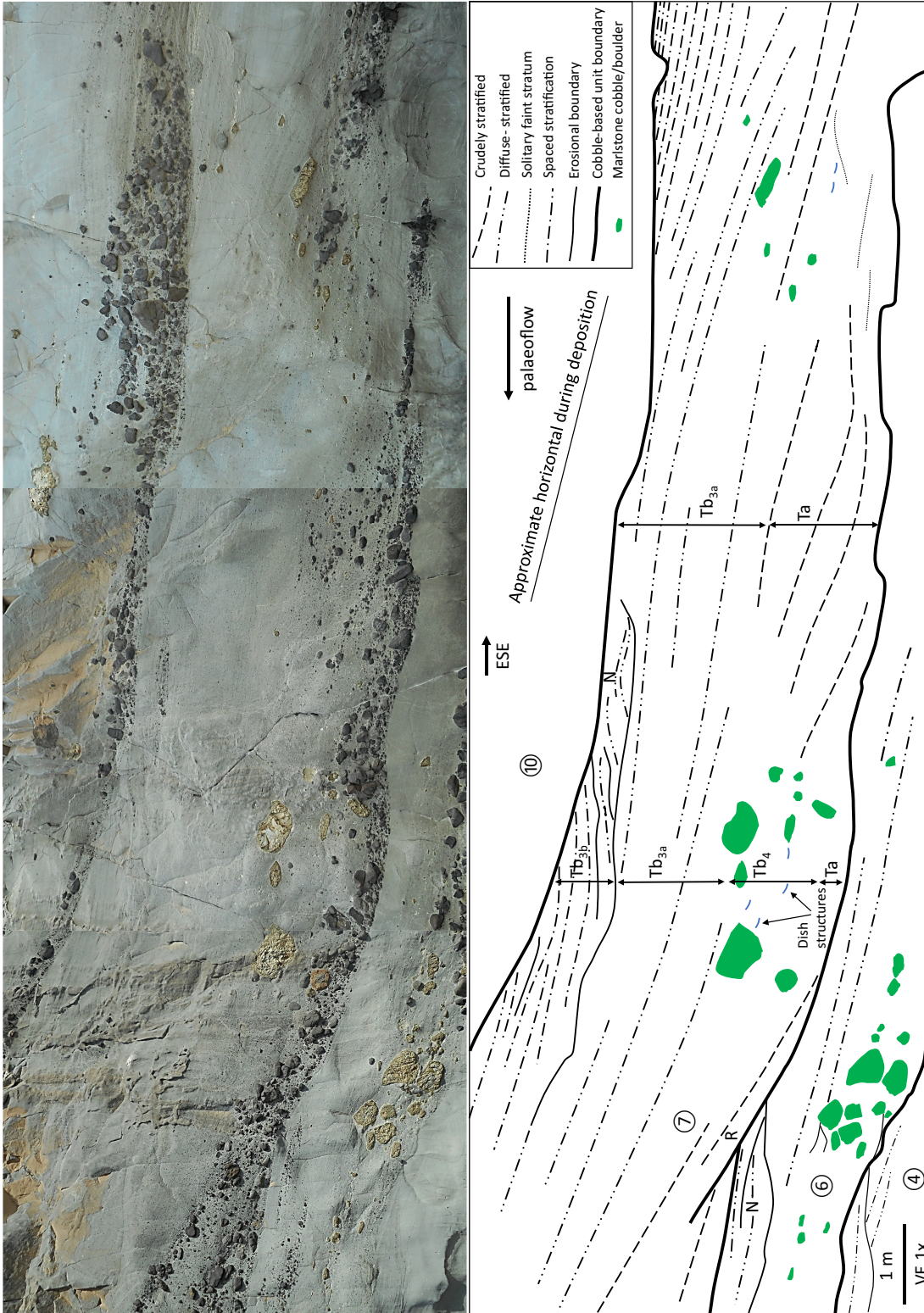
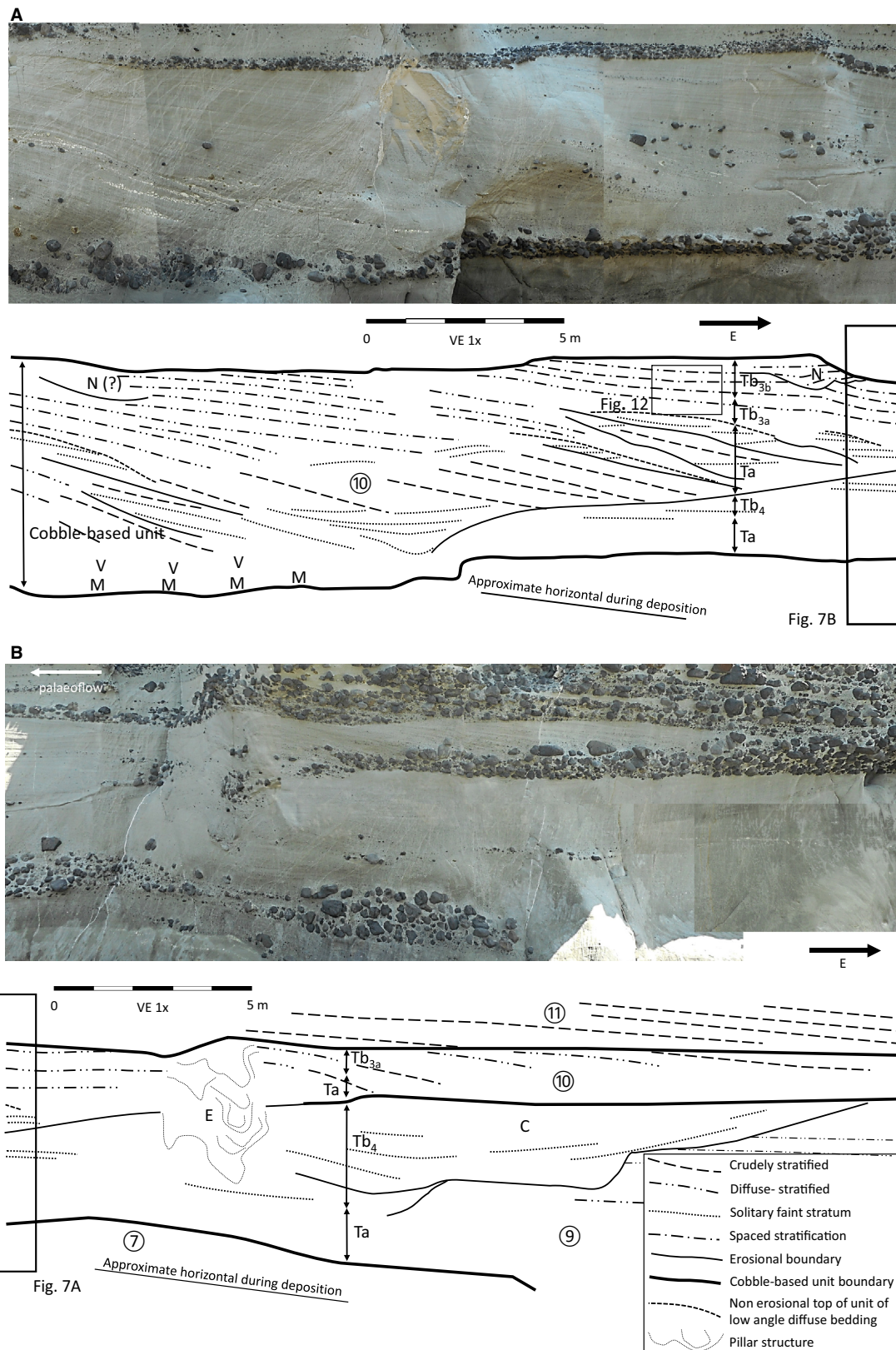
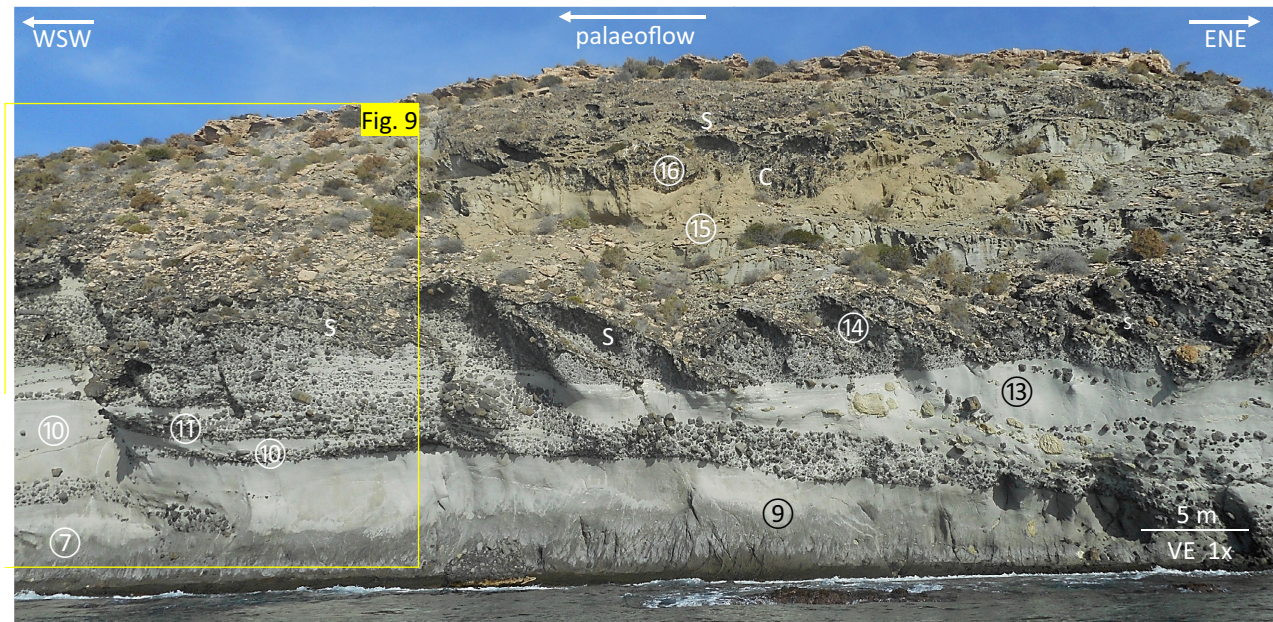


Fig. 6. Architecture of cobble-based sedimentary units 6 and 7 (detail from Fig. 9). 'N' denotes lens-shaped nucleus of antidune structure. 'R' denotes reactivation marks.



**Fig. 7.** (A) and (B) Complex architecture of CB-units 9 and 10 (detail from Fig. 9). ‘C’ denotes massive sand layer mentioned in text. ‘N’ denotes antidune structure. ‘E’ denotes pillar structure. ‘M’ denotes structureless sand pocket. ‘V’ denotes preferential near-vertical orientation of cobble long axes.



**Fig. 8.** Low-angle crudely cross-bedded layers in CB-units 14 and 15. 'C' denotes contorted bedding. 'S' denotes crude sigmoidal cross-bedding. See Fig. 3 for location.

## INTERPRETATION

### Cyclic step origin

By far most large-scale cross-stratification identified at outcrop has an easterly dip direction. At first sight this may suggest deposition by large dunes in a unidirectional flow. However, the cross-bedding was not produced by slip-face avalanche processes typical of migrating dunes, because the dip of individual cross-strata has values well below the angle of repose. Moreover, in contrast to the inversely graded, well-defined strata that characterize cross-beds produced by grainflow avalanches down dune slip faces (Kleinhan, 2004), the volcanoclastic cross-beds have a crude or diffuse appearance with ill-defined strata boundaries. In individual sets the volcanoclastic cross-strata attain their highest dip angles near the unit base, with a gradual reduction in inclination upward through the unit until they more or less parallel the unit boundaries, suggesting an almost complete preservation of the original bedforms. However, the typical tripartite division of a nearly complete dune deposit consisting of a fine-grained, ripple-laminated bottomset followed by high-angle foresets that pass upward through a distinct brinkpoint to a low-angle stratified topset

(Boersma, 1967; Martinius & Berg, 2011; Martinius *et al.*, 2015) is not found.

The cyclic steps that are described from submarine slopes of insular volcanoes show a large variation in bedform wavelength (36 to 1650 m) and height (1 to 200 m; Casalbore *et al.*, 2021). Seismic profiles across fields of cyclic steps on submarine slopes of volcanoes (Pope *et al.*, 2018) and comparable submarine settings show the sigmoid-shaped backset structures produced by their upslope migration during turbidity current events (e.g. Migeon *et al.*, 2000; Zhong *et al.*, 2015; Vendettuoli *et al.*, 2019). The angle of climb of the cyclic-step bedforms often is so high that their stoss sides are completely preserved, a condition termed fully depositional in the classification of cyclic step depositional signatures by Slooman & Cartigny (2020). In cases where subsequent erosion of the stoss-side of the cyclic steps occurs, classified as partly depositional, sets produced by the upslope migrating cyclic steps are tabular in longitudinal, flow-parallel section. This set shape distinguishes cyclic-step deposits from the more chaotic geometries produced by other up-current migrating supercritical bedforms (antidunes and chutes-and-pools (Cartigny *et al.*, 2014; Ono & Plink-Björklund, 2018; Slooman *et al.*, 2021). The tabular bounding surfaces with internal

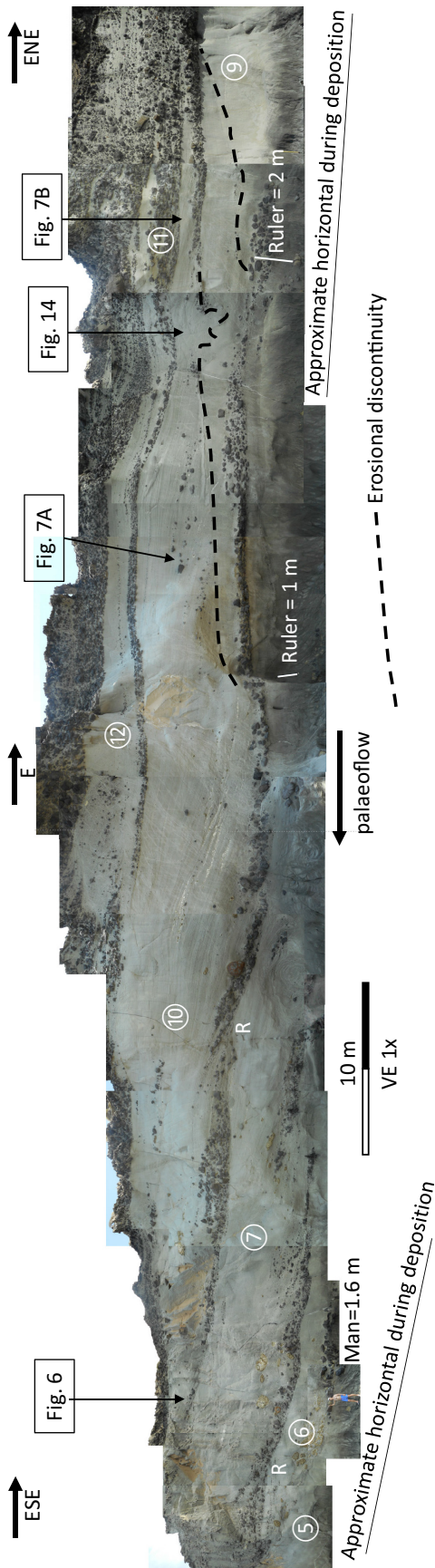


**Fig. 9.** Photomosaic of the central part of the cliff section. Circled numbers identify specific cobble-based units. ‘R’ indicates reactivation marks. See Fig. 3 for location.

sigmoidal stratification are consistent with observations from the CB-units of the Cuatro Calas outcrop, which therefore are interpreted as cyclic-step deposits generated by high-density flows transporting abundant coarse-grained material. Thus, the CB-units are produced by cyclic steps and the cross-strata at the base of the units are backsets. Corrected for tectonic tilt the cyclic steps producing these backsets climbed in an east to north-easterly direction, opposite to the downslope direction of the formative sediment density flows.

To avoid any misinterpretation in the following discussion, stratal dip and geometry are always corrected for tectonic influence. In photographic panels a straight line is added showing the estimated palaeohorizontal plane at time of deposition. This is based on a number of consistent indicators: (i) an average slope of 12° for the lower part of backsets of partly depositional cyclic step deposits in flow-parallel sections, derived from a seismic line over cyclic steps of a modern submarine volcanic slope (Pope *et al.*, 2018, fig. 5f); (ii) corrected for this palaeohorizontal reconstruction, the diffuse stratification shows a subhorizontal inclination (see Figs 9 to 12), in agreement with the horizontal to very low angle surface that characterizes the upper part of the cyclic-step stoss side (Slootman & Cartigny, 2020). The estimated palaeohorizontal surface implies an angle of climb of the cobble-based backsets of approximately 4° to 6°. Additional support for the reconstructed paleohorizontal surface comes from two indicators of horizontality: (iii) the orientation of dish structures (Fig. 6); and (iv) the preferential inclination of long of clast axes in cobble layers above pockets of structureless sand (Fig. 7A). Dish structures are currently interpreted as having formed during the dewatering of very rapidly deposited sediment and they are inferred to have assumed a preferentially horizontal orientation at time of formation (e.g. Lowe & LoPiccolo, 1974; Lowe, 1975; Mills, 1983). At some locations below the cobble layer of CB-unit 10, a structureless sand pocket is present above the erosional unit boundary, while corrected for the assumed tectonic tilt the long axes of the clasts in the cobble layer above it show a preferred vertical orientation (Fig. 7A: indicated by ‘M’ and ‘V’). Subvertical clast imbrication is occasionally described from deposits of debris flows and high-density underflows, not yet entirely understood in terms of its origin but in some studies attributed to upward expulsion of water during sedimentation (Sohn

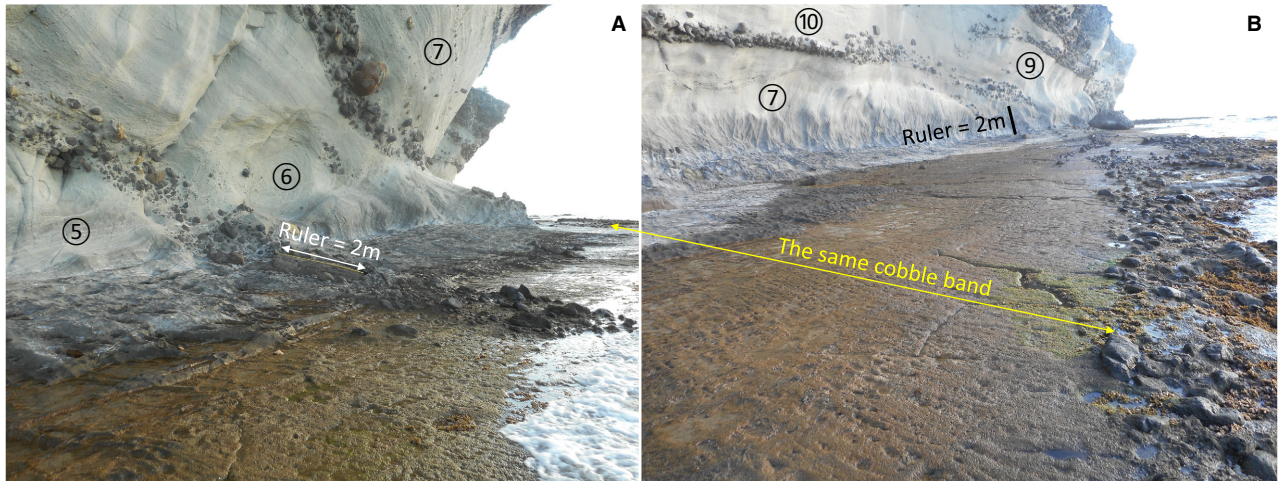


**Fig. 10.** Cobble-bearing divisions at the base of CB-units 7 and 9. Some boulders are also evident in the cliff wall and the abrasion platform. (A) Ruler rests on the largest andesite clast of the outcrop, with a long axis measuring 2 m. (B) Cobble band at the base of CB-unit 9 can be followed several tens of metres in the abrasion platform.

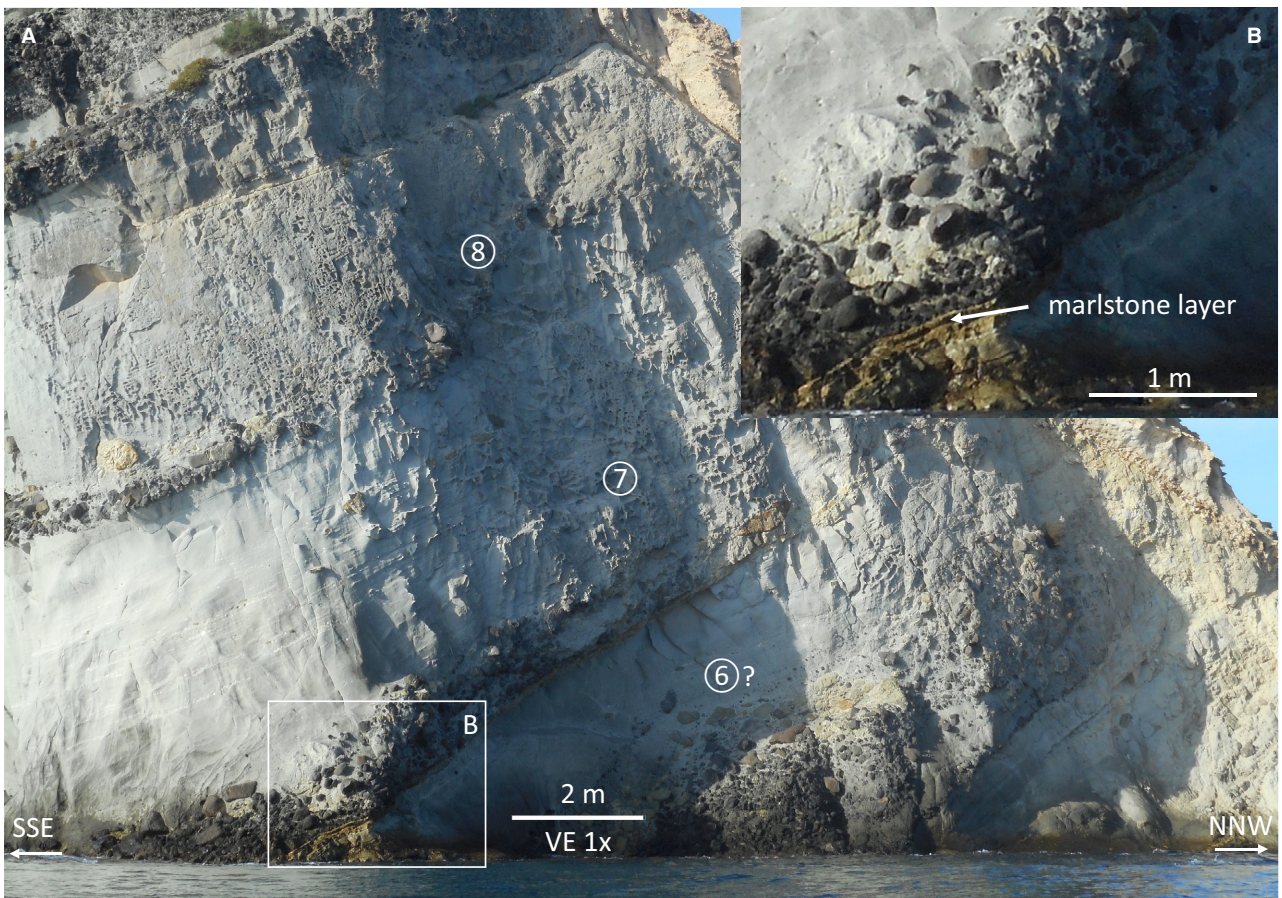


**Fig. 11.** Marl layer between cyclic step deposits, viewed in almost flow-perpendicular section. Palaeoflow direction into the photograph. See Fig. 2B satellite image for location.

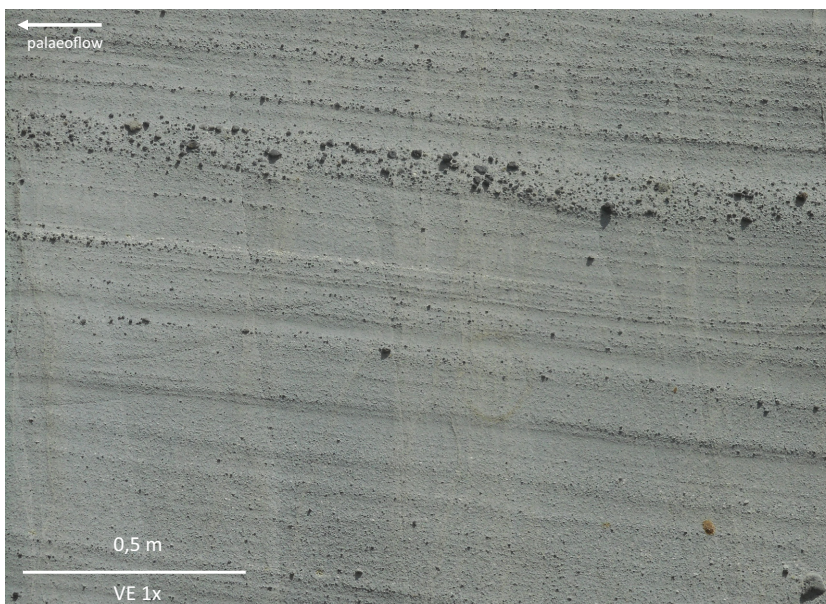


**Fig. 12.** Diffuse stratification passing upward into spaced stratification (detail from Fig. 7A).

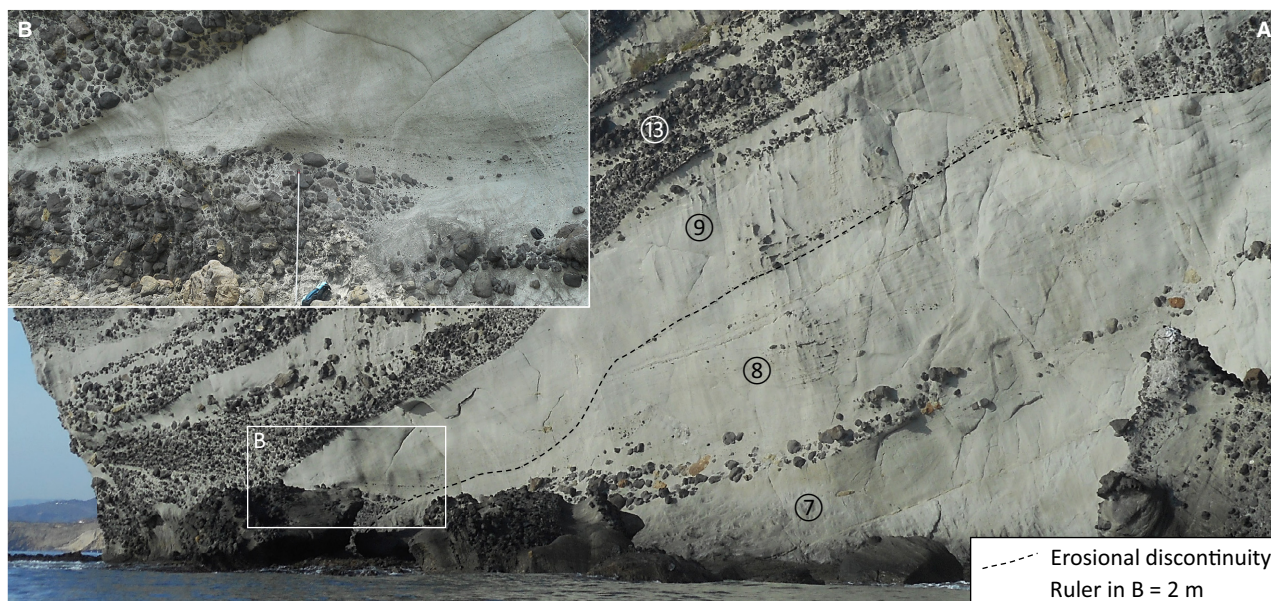


**Fig. 13.** Partly exposed cyclic step trough-fill. Palaeoflow oriented obliquely to the left in the view direction. See Fig. 2B satellite image for location.

*et al.*, 1999; Mulder, 2011; Postma *et al.*, 2014). Similar assemblages of vertical clast fabrics above a massive sand pocket can be observed at the base of hydraulic-jump-related deposits in successions of the ancient Buho Canyon in southern Spain (Postma *et al.*, 2014, fig. 7C). It is speculated here that these assemblages result from a process of vertical grain segregation caused by the ‘Brazil nut

effect’ (Clement *et al.*, 2010; Liao & Hsiao, 2016), also known as kinematic sieving, induced by vibrations in the wake of the hydraulic jump.

### Sedimentary architecture of CB-units

In this section, first the attention is focused on the CB-units with a relatively simple

architecture, comprising a single sigmoidal structure, such as CB-unit 7 in the right part of Fig. 6. This is followed by a discussion of architecturally more complex units.

### Simple CB-units

Although the depositional architecture of these CB-units has much in common with the succession presented by Postma *et al.* (2014), summarized here in the *Introduction* chapter, there are a number of differences. To start with the lowermost division (Ta), in the entire outcrop only one flame structure was found (Fig. 4 and Data S1, base of CB-unit 2). The coarse-tail graded and structureless divisions Ta and Tb<sub>4</sub> appear to be transitional. They show a very variable thickness, even over short distances in the same set (Figs 6 and 7). At some locations the structureless Tb<sub>4</sub> division is completely missing and crude backset strata are visible right from the very base of the set (Fig. 6, CB-unit 7).

The variable thickness of the structureless Ta and Tb<sub>4</sub> divisions may be related to changes in the strength of the hydraulic jump. Rapid deposition under low flow shear in the hydraulic jump zone would be expected to produce a massive coarse-tail graded deposit (Postma *et al.*, 2009). However, with increasing strength of the hydraulic jump, the base of CB-units scoured deeper, countering rapid aggradation in correspondence to the hydraulic jump. Instead, the crude bedding directly overlies the lower bounding surface and encompasses the normal graded Ta division. Such a deepening and related absence of structureless deposits is shown in Fig. 6: After being scoured to a greater depth (upstream of R), with crude bedding toe-lapping the unit's bounding surface, the base of CB-unit 7 is observed to rise. This rise is interpreted as the result of a decrease in the intensity of the hydraulic jump, which resulted in an increased aggradation rate and in the consequential appearance of a deposit without stratification above the basal cobble-bed (Tb<sub>4</sub>) with some dish structures. This succession is repeated in the right part of Fig. 6.

For unknown reasons the crude low angle bedding at the base of the CB-units is lacking in the lower part of the volcanoclastic succession and the coarse-tail normally-graded division (Ta) here is everywhere represented by a structureless deposit (CB-units 1 to 3, see Fig. 4 and Data S1). The average thickness of the diffuse strata tends to decrease in the upper parts of the sets, which fits the decrease in aggradation rate

expected on the downstream part of the stoss side. As can be seen in Fig. 12, the diffuse strata lack the inverse grading that characterizes the spaced stratification (Tb<sub>3b</sub>) facies as presented in the model of Postma & Cartigny, 2014; Fig. 1). Non-graded crude backsets and overlying diffuse stratification therefore are both classified as belonging to the crude stratification (Tb<sub>3a</sub>) facies. Upward through the unit succession, the diffuse strata become gradually less thick, more regular and somewhat sharper outlined (Fig. 6, right part; Fig. 12). This type of bedding here is considered spaced stratification as described by Hiscott & Middleton (1979) and Hiscott (1994), although the typical inverse grading of individual strata was not observed. However, this does not prevent classification of this facies as spaced stratification (Tb<sub>3b</sub>), because this type of bedding sometimes appears not to be inversely graded (Sumner *et al.*, 2012). Planar lamination <0.5 cm (Tb<sub>2</sub>) forming the upper division in the model of Postma & Cartigny (2014; Fig. 1) has not been found anywhere in the outcrop.

Because the textural grading in the lowermost Bouma division (Ta) is recognizable at outcrop also where sedimentary structures are not well-exposed, it is given priority in the facies classification. Thus, in the case that a coarse-tail normal graded layer consists of crude backsets it is not classified as Tb<sub>3a</sub>, according to its sedimentary structures, but as Ta, based on its textural grading.

### Complex CB-units

The architecture of CB-units may be complicated by superimposed sigmoidal cross-bedding without a cobble-base (Fig. 4: CB-units 1, 2, 4 and 9; Fig. 5: CB-unit 4, Fig. 6: CB-units 6 and 7; Fig. 7: CB-unit 10; and Fig. 13: CB-unit 9). These secondary structures as described in the previous section either represent cyclic-step trough-fills, or were produced by hydraulic jumps and related bedforms that formed superimposed on the stoss side of the larger master cyclic steps. Three types of secondary, superimposed structures are distinguished here: cyclic step trough-fills, superimposed cyclic step backsets and downflow-migrating antidune structures.

*Cyclic-step trough-fills.* The excellent exposure conditions allow a full reconstruction of a fill structure in CB-unit 10, presented in detail in Fig. 7. In Fig. 14, five stages are distinguished. The density-flow event during which the fill

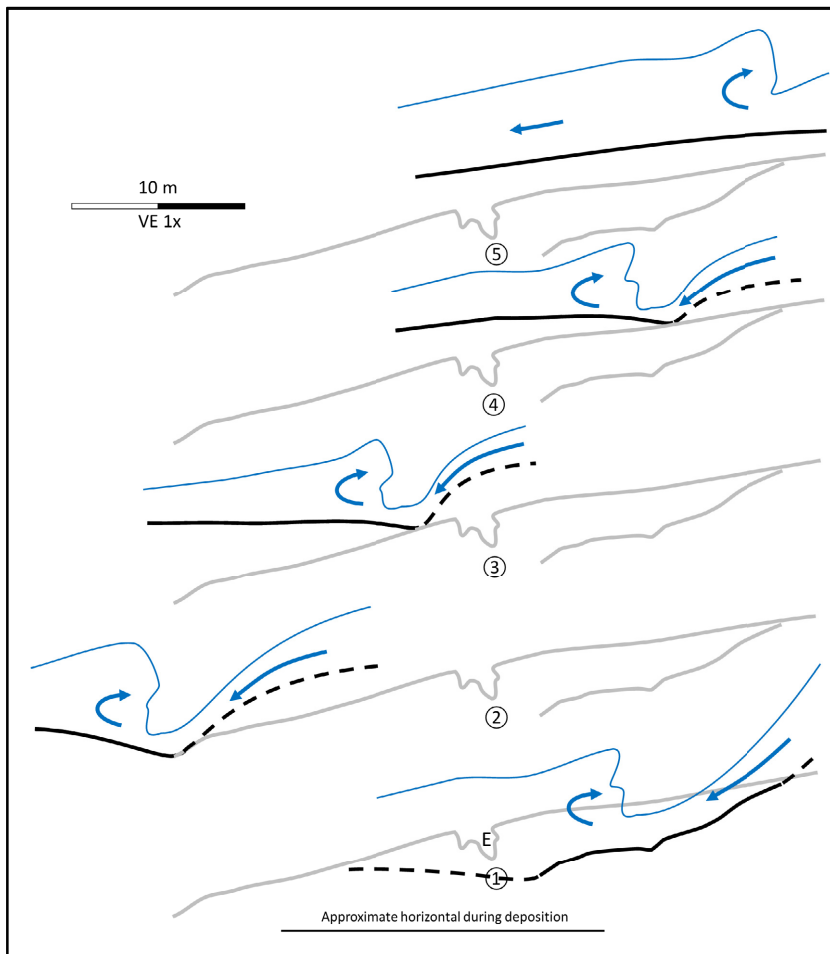


**Fig. 14.** Reconstruction of stages (①, ②, ③, etc.) of infilling of the cyclic step trough from which CB-unit 10 is built-up. The grey line denotes the erosional discontinuity indicated in Figs 7 and 9. 'E' denotes deformation pocket (see also Fig. 7B). The solid line provides a morphological reconstruction of the original bedform profile based on preserved sedimentary structures. The dashed black line provides an inferred morphological reconstruction of the bedform profile. The blue line provides an inferred reconstruction of the hydraulic profile of the high-density flow. For details of sedimentary structures, see Fig. 7.

structure formed possibly started at the beginning of the scour indicated by 'R' in Fig. 9. Stage 1 represents the beginning of a period during which the high-density underflow over the cyclic steps was reduced considerably in strength. This is documented by the preservation of the lowermost part of the steep lee-side of the cyclic step (upslope part of grey line in Fig. 14). Between stages 1 and 2, the upslope migration of the lee-side slope was interrupted by a downslope migration of about 27 m, as evidenced by the length of the internal scour surface. This may be explained by a temporal collapse of the hydraulic jump due to a sudden reduction in the strength of the density flow. The faintly bedded massive sand (indicated by 'C' in Fig. 7B) that accompanied this shift reflects an extremely rapid aggradation rate under conditions of low flow shear (Sumner *et al.*, 2008; Talling *et al.*, 2012; Van den Berg *et al.*, 2017). After adapting to this temporary interruption, the hydraulic jump revived at a position farther downstream. Some resemblance

is found in small backset structures at the base of preserved lee-sides of much larger cyclic steps described by Ghienne *et al.* (2020) from Quaternary upper delta-slope sands in Québec (Canada), and interpreted as being produced during waning-flow conditions. However, those backsets were formed directly on the lee-side of the master cyclic-step bedform and die out at short distances, marking the end of the sediment density flow event. Contrary to that, in the case discussed here, during stages 2 to 4 (Fig. 14) the flow and the counter-current upslope migration of the hydraulic jump continued, which resulted in the deposition of convex-upward, diffuse backset stratification infilling the trough of the master cyclic-step bedform. Minor erosional discordances within these low-angle structures bound faintly stratified wedges (Fig. 7A), that locally also occur at the base of simple CB-units (Fig. 7A, left side), and resemble those produced in flume experiments using a mixture of sand and fine gravel (Ono *et al.*, 2021). These were formed by successive pulses of gravel



sedimentation that accreted on a small mound, forming low-angle foreset structures on its downstream side. Although in the outcrop the wedges mainly consist of coarse-grained sand instead of fine gravel as in the experiments, it is fair to assume that their formation mechanisms are comparable. Therefore, these are also considered as an expression of the inherent instability of the hydraulic jump. The assumption that the reduced flow strength continued during the filling of the cyclic-step trough is supported by the fact that no cobbles laid down on the erosion surface formed during stages 3 to 4, as this suggests that the density flow was not strong enough to transport gravel clasts. Similarly, the reappearance and thickening of the cobble layer at the base of the erosional boundary in stages 4 and 5 indicates that the flow regained strength. The deformation pocket indicated by 'E' in Figs 7B and 14 is interpreted as a water-escape pillar structure (see also Postma, 1983). The trough-fill documents the end of CB-unit 10. Just before the start of the filling process, the trough in front of the cyclic step that formed this unit eroded CB-unit 9 remarkably only down to its lower bounding surface. This implies that, in this case, the climbing angle of the cyclic step was the same as the seafloor inclination. One might expect that the density flow event that caused the trough-fill generated similar reactions in nearby cyclic-step troughs: this is exactly documented by the presence of a similar infill at the same chronostratigraphic level preserved in the ESE facing part of the cliff (Figs 3 and 13A). In this fill, that is shown in oblique section with respect to the cross-bed dip-direction, the reduction of flow capacity is also reflected by the absence of the basal cobble-layer (Fig. 13A). The weakening of flow strength that initiated the trough-fill process is well-illustrated by the sudden transition of cobble-dominated to sand-dominated crude cross-stratification at the beginning of the fill structure (Fig. 13B). The distance between the start of both fills is about 170 m, which thus approximates the length of the cyclic step that produced CB-unit 9. Note that the two trough-fills are time-equivalent but belong to successive CB-units (Fig. 3: CB-units 8, 9 and 10), because they represent successive bedforms in a field of cyclic steps.

No published sedimentary structures show similarity with the cyclic-step trough-fill described here, with the exception of the 'build-up-and-fill structures' described by Slooman *et al.* (2021) from a Pleistocene submarine

carbonate slope. Those examples also refer to very large supercritical bedforms but have a different origin. They are thought to have formed in temporal cycles of large chutes-and-pools and antidunes in a density flow that, apart from minor short-term variations, was substantially steady. In contrast to the instability of chutes-and-pools, cyclic steps are stable features in steady flows. The trough-fill structures described here document the bedform response to a dramatic temporal reduction of the strength of the density flow and to a related change in the hydraulic jumps responsible for the infill of troughs between the cyclic steps. In contrast to the frequent occurrence of build-up-and-fill structures in the facies described by Slooman *et al.* (2021), only two synchronous trough-fill structures can be observed in the Cuatro Calas outcrop. These fills lack the standing wave to antidune build-up of build-up-and-fill structures, whereas the latter structures lack any indication of temporal downstream shifts of the hydraulic jump.

*Superimposed cyclic steps.* Some secondary structures with metric thickness and up to tens of metres long in flow-parallel oriented sections show a similar regular sigmoidal cross-bedding as the larger cobble-based cyclic steps (Fig. 5 and Data S1), suggesting that they were possibly formed by smaller, cyclic steps superimposed on master bedforms. So far, evidence for such superposition has not been reported in the literature. The equilibrium length of cyclic steps increases with flow discharge (Cartigny *et al.*, 2011). It is supposed here that, in analogy with the development of superimposed small dunes on large relict dunes with decreasing discharge in deep rivers (e.g. Allen & Collinson, 1974), superimposed cyclic-step backsets represent a change to smaller cyclic-step lengths, matching a reduced discharge of the density underflow. Unfortunately, all of these secondary backset structures are less well exposed, and this aspect therefore could not be investigated in more detail.

*Superimposed downflow migrating antidunes.* The 1 to 2 m thick and 3 to 10 m wide structures that can be observed at the top of CB-units 6, 7 and 10 (Figs 6 and 7A) are interpreted to represent downstream-migrating antidunes. The spoon-shaped scours and lens structures at their base followed by downstream low-angle cross-bedding with erosional discontinuities are very

similar to descriptions offered by Fielding (2006), Ito (2010), Lang & Winsemann (2013), Fedele *et al.* (2016), Lang *et al.* (2017) and Cornard & Pickering (2019). Observations from flume experiments confirm that antidunes can be formed superimposed on the stoss side of cyclic steps (Cartigny *et al.*, 2014). The preservation of the lens and foreset signature is indicative for conditions of extremely rapid aggradation (Cartigny *et al.*, 2014; Slootman & Cartigny, 2020). Numerical simulations indicate that in nature antidunes occur in association with cyclic steps, developing wavelengths at least one order of magnitude shorter than those of cyclic steps (Kostic, 2011). Evidence for the presence of antidunes superimposed on cyclic steps in modern submarine environments is restricted to some series of very large steps in fine-grained sediment (Kostic, 2014; Zhong *et al.*, 2015), with antidune wavelengths exceeding 2 km superimposed on much larger cyclic steps. These extremely large bedforms represent conditions of fine bed material formed under supposedly very thick and non-stratified density flow. Such conditions are very different from those inferred for the thinner and denser, stratified underflows over coarse sand and gravel that created the much smaller cyclic steps of the Cuatro Calas volcanoclastics. For these conditions, information is lacking from any modern equivalent. In the dense-saline underflow experiments with fine-grained and medium-grained sand by Fedele *et al.* (2016), downstream migrating antidunes appeared at densimetric Froude numbers ranging between 1.2 and 1.8. They were shown to be relatively short in wavelength compared to those generated for similar Froude conditions in very fine-grained sediment. The antidune structures in the photographic panel displayed in Fig. 6 documents a growth in amplitude and a downstream extension of preserved foresets starting from a nucleus indicated by 'N' in Fig. 6. This points to a downstream migration of the antidunes. After some distance, the downstream-directed foresets lose their identity as they parallel the diffuse bedding of the stoss-side deposits of the cyclic step, indicating that the antidunes reached a length of 5 to 10 m. The growth in amplitude suggests an unstable antidune origin. In free surface flows unstable antidunes, as defined by Cartigny *et al.* (2014), commonly form trains of bed waves that grow and dissipate cyclically in alternation with (quasi) planar bed in a temporal cycle, as described by Kennedy (1961), Middleton (1965)

and Schumm *et al.* (1982). It is not yet known whether this morphodynamic cycle applies also for downflow migrating antidunes under natural high-density underflows, and over what time-scales. The saline underflow experiments of Fedele *et al.* (2016) suggest that downstream migrating antidunes are more stable features in density flows. Extrapolation of the stability diagram of Fedele *et al.* (2016) for dense underflows to the very coarse sand suggests that short downflow migrating antidunes like those found superimposed on the large cyclic steps of the Cuatro Calas volcanoclastics may form within the range 1.5 to 2.0 of the densimetric Froude number. Following Cartigny *et al.* (2014), it is thought plausible that with increasing flow strength these antidunes can form an incipient stage in the development of the backsets of the smaller secondary cyclic steps found within the CB-units. Alternatively, their presence at the top of the CB-units suggests a linkage to waning-flow conditions (see Dietrich *et al.*, 2016).

### Size and shape of the inferred cyclic steps

The tabular geometry of the sand-dominated CB-units indicates that the planform crest shape of their formative cyclic steps must have been straight to slightly sinuous. With their straight set boundaries in a flow-parallel and perpendicular section the geometry of these straight-crested cyclic steps deposits differs from the lenticular-shaped bodies produced by crescentic cyclic steps (Postma *et al.*, 2014; Ghienne *et al.*, 2020; Englert *et al.*, 2021). In the case of fully depositional cyclic steps, their height and length is easily obtained from preserved structures in outcrop or seismic images. This is also the case when formsets are preserved, such as described by Ponce & Carmona (2011) from the north-east Atlantic coast of Tierra del Fuego, Argentina. In the case of partly depositional cyclic steps, such as in the Cuatro Calas successions, such information is not available and bedform dimensions can only be estimated from set height,  $S$ , and cyclic steps climbing angle,  $\alpha$ , combined with the palaeoslope of the seafloor,  $\beta$ . Here, a simple method is presented to estimate cyclic-step length and height from these data.

Series of cyclic steps in flow-parallel cross-section resemble staircase treads (Fig. 15A). The height of one step in a staircase depends on its length and on the inclination of the

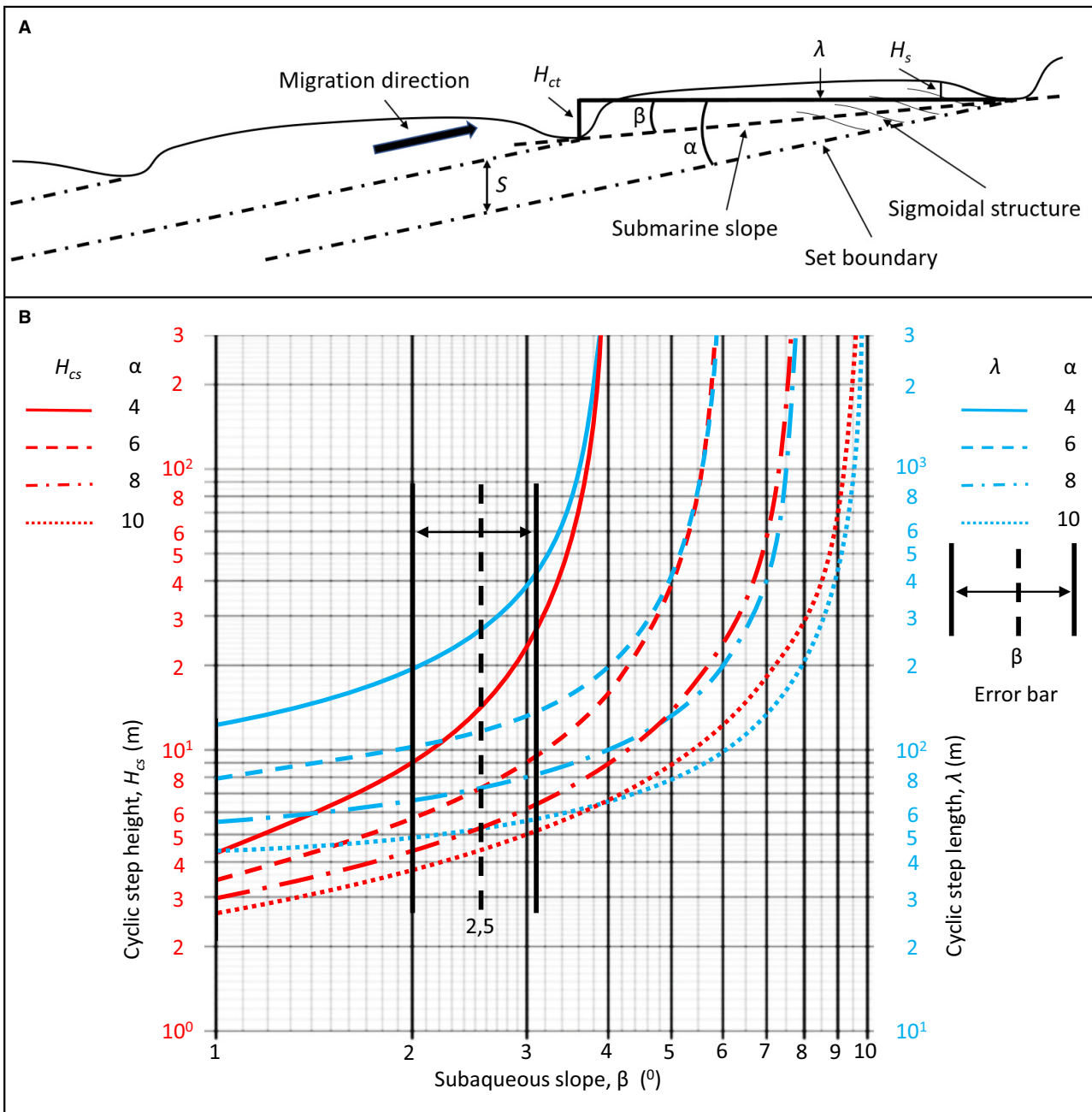


**Fig. 15.** Derivation of bedform height and length from deposits of partially depositional, convex to straight-crested cyclic steps. (A) Triangular schematization of cyclic step geometry.  $H_{ct}$  and  $\lambda$  = height and length of a triangular-shaped cyclic step.  $H_s$  = thickness of completely preserved sigmoidal backset structure or coarse-tail normally graded-layer.  $S$  = cyclic step set height.  $\alpha$  = cyclic step climbing angle.  $\beta$  = palaeo area slope. (B) Computational results for  $S = 7$  m and  $H_s = 2$  m for various combinations of  $\alpha$  and  $\beta$ . The error bar shows sensitivity for a 25% deviation from an assumed subaqueous slope  $\beta = 2.5$ .

seafloor. For such schematically triangular cyclic steps, straight-crested in plan view and aggrading with a constant climbing angle the

height,  $H_{ct}$ , and length,  $\lambda$ , of a triangular-shaped cyclic step, can be estimated as follows (see also Fig. 15A):

$$H_{ct} = \lambda \tan \beta \quad (\text{m}) \quad (1)$$

and:

$$S = \lambda (\tan \alpha - \tan \beta) \quad (\text{m}) \quad (2)$$

combining Eq. 1 and Eq. 2 gives:

$$H_{ct} = \tan \beta (\tan \alpha - \tan \beta)^{-1} S \quad (\text{m}) \quad (3)$$

Note that the values of  $\lambda$  and  $H_{ct}$  are proportional to the set height,  $S$ . In reality the summit of a cyclic step is not flat and horizontal, but elevated above the upslope situated trough. The minimum elevation is provided by the height of the preserved sigmoidal structure,  $H_s$ , above the horizontal surface,  $\lambda$ , as drawn in Fig. 15A. In the case that this backset structure is not identifiable at outcrop, the thickness of the coarse-tail graded layer can be used as a proxy.  $H_s + H_{ct}$  gives the cyclic step height,  $H_{cs}$ :

$$H_{cs} = \tan \beta (\tan \alpha - \tan \beta)^{-1} S + H_s \quad (\text{m}) \quad (4)$$

Estimates of the seafloor gradient unfortunately cannot be derived from the deposits, and therefore remain rather uncertain. Evidence from fields of sinuous to straight-crested cyclic steps from modern volcanic islands indicates seafloor slopes,  $\beta$ , between  $1^\circ$  and  $8^\circ$  (Casalbore *et al.*, 2014, 2021; Pope *et al.*, 2018; Santos *et al.*, 2019). The latter authors mention an average of  $2.5^\circ$ , which is adopted here, because the climbing rate,  $\alpha$ , is only  $4$  to  $6^\circ$  and the difference with  $\beta$  must at least be several degrees to produce sedimentary units with a thickness of more than 10 m (Fig. 15B). With these estimations and applying Eq. 2, a schematized triangular cyclic-step height,  $H_{ct} = 8.5$  m ( $\alpha = 6^\circ$ ) and  $H_{ct} = 20$  m ( $\alpha = 4^\circ$ ) is calculated for the largest CB-unit that is not affected by secondary backset structures (Fig. 4: CB-unit 2). With an arbitrary 2 m thickness of the coarse-tail normal graded layer added (Eq. 4) the estimated cyclic-step height,  $H_{cs}$ , and length,  $\lambda$ , is between 10.5 to 22.0 m and 195 to 457 m, respectively. The CB-units that can be followed over large distances in the outcrop vary in thickness from 4 to 12 m. For the smallest set thickness  $S = 4$  m the procedure above results in a bedform length,  $\lambda$ , and a cyclic-step height,  $H_{cs}$ , between 65 to 152 m and 4.8 to 8.7 m, respectively. As the subaqueous slope,  $\beta$ , cannot be determined from preserved deposits the value used for calculations is to be considered a crude estimate. In Fig. 15B the sensitivity of the assumed value for errors is shown for various values of the set

climbing inclination  $\alpha$ . The sensitivity increases as the difference between the value of  $\alpha$  and  $\beta$  decreases, eventually approaching infinity. For the cyclic-step parameter conditions considered in Fig. 15B an error bar is drawn for a 25% deviation from  $\beta = 2.5$ . For this and any other deviation the sensitivity can be easily found in the graph by applying the appropriate error bar to a selected value of  $\beta$ .

The sand-dominated cyclic-step deposits are followed upward by sigmoidal backsets that consist entirely of gravel (Fig. 4: above 52 m; Fig. 8: CB-unit 14). The crude bedding of these gravel backsets has a higher angle because in the wake of the hydraulic jump the gravel settles over shorter distances than sand (Slootman & Cartigny, 2020). The trough-shaped backsets in the CB-units at the top of the volcanoclastic succession suggest a more three-dimensional shape for the cyclic steps that created them.

## Palaeoenvironment

Because the pebbles and cobbles at the base of CB-units are preferentially deposited in the wake behind the hydraulic jumps, the density flows gradually must have lost them during their downslope movement, and more distal deposits will therefore lack the concentrated cobble layers at their base. The fact that backset strata in the upper part of the succession consist completely of cobbles embedded in a matrix of fine gravel and coarse sand (Fig. 3 – above CB-unit 10 – and Fig. 8) therefore points to deposition at the proximal end of a bedform field. As discussed earlier, this is possibly a coastal or shallow-water area as supported by the palaeogeographic reconstruction. Unfortunately, the hypothesis of upward coarsening in a shallow water setting, proximal to the origin of the density flows cannot be checked with data of modern environments because the present knowledge of cyclic steps on submarine slopes mainly refers to their occurrence, morphology and seismic appearance, while systematic textural data are still lacking.

Submarine slopes of volcanoes tend to become steeper in shallow water (e.g. Casalbore *et al.*, 2021). This tendency is also evident in the Cuatro Calas succession. For the lower part a submarine slope  $\beta = 2.5^\circ$  was assumed. In CB-units 8 to 10, the submarine slope equals the  $4^\circ$  to  $6^\circ$  inclination of the set climbing. A marked further increase in set climbing starts with CB-unit 14 (Fig. 8), coincident with the transition from sand-dominated to gravel-dominated CB-units. If

the rate of climbing is proportional to the inclination of the submarine slope this would imply an increase of related specific flow energy as well. This is supported by the fact that coarser-grained cyclic steps tend to occur on a higher slope gradient (Dietrich *et al.*, 2016). On submarine volcanic slopes steeper gradients generally mean a more shallow bathymetric setting. The increase in energetic conditions goes along with a difference in plan view of the cyclic steps. Cyclic steps generally assume a crescentic shape in channel conduits, whereas the two-dimensional plan view inferred for the large cobble-based cyclic steps indicates an unconfined setting (Symons *et al.*, 2016; Pope *et al.*, 2018). This suggests that, in analogy with subaqueous dunes of the lower flow regime (Southard & Boguchwal, 1990; Best & Fielding, 2019), a two-dimensional plan view of cyclic steps is an expression of less energetic conditions.

The outcrop-based facies model of Postma & Cartigny (2014) mainly applies to confined conduits such as submarine canyons (Postma *et al.*, 2014; Lang *et al.*, 2017; Ono & Plink-Björklund, 2018) and delta-slope channels (Ghienne *et al.*, 2020), where cyclic steps are typically crescent-shaped with limbs pointing downslope. At some point the conduit channels widen and gradients are reduced (Casalbore *et al.*, 2014; Santos *et al.*, 2019). In these unconfined settings cyclic steps feature sinuous or straight outlines (Casalbore *et al.*, 2014, 2021; Zhong *et al.*, 2015; Symons *et al.*, 2016; Pope *et al.*, 2018), like those of the sand-dominated CB-units discussed in this paper. Bedforms with wave height of 1 to 5 m and wavelength of tens or few hundreds of metres, similar to those that formed the cobble-based cyclic-step deposits discussed here, have been reported from the upper part of submarine flanks of islands of in the Aeolian Archipelago (Romagnoli *et al.*, 2012; Casalbore *et al.*, 2016a; Casalbore *et al.*, 2018) and Ventotene (Casalbore *et al.*, 2016b) in the Mediterranean Sea, Terceira (Chiocci *et al.*, 2012) in the North Atlantic and Tanna island in the South Pacific Ocean (Clare *et al.*, 2018). In all of these settings, they are related to shallow (first 200 to 400 m water depth) and flat-bottomed channels, except for Salina, one of the Aeolian islands, where similar bedforms also form at the end of the channels on small fan-shaped features (see also Casalbore *et al.*, 2021). It is important to remember that the Cuatro Calas case possibly refers to the submarine slope of a volcano that partly or completely rose from a shallow sea, a different

setting from the investigated submarine slopes of deep sea-based insular volcanoes.

### Reactivation markers of cyclic-step activity

Pebble to boulder-sized green marlstone clasts can be observed locally, generally within Tb<sub>3a</sub> facies (Figs 5, 6, 8 and 11). These are considered to be rip-up clasts originated from mud layers that accumulated on the cyclic-step bedforms during long periods between turbidity current events. The preservation of mudstone or marlstone clasts in cyclic-step deposits is a common phenomenon (Postma *et al.*, 2014, 2021; Lang *et al.*, 2017), but generally conclusive evidence of a rip-up origin from mud blankets that accumulated between density flow events is lacking. In the Cuatro Calas case, however, it is sure that the marlstone clasts originated from such blankets, because in a volcanic environment other sources for such lithologies are simply not available. At one location, at the north-east facing part of the outcrop, the forces exerted by turbidity currents obviously were not strong enough to mobilize the mud layer, and a part of the original marl blanket covering the deepest part of a bedform trough remained *in situ* (Fig. 11). Seismic profiles over modern cyclic steps show little evidence for discontinuities between two consecutive density flow events. Either cyclic steps simply migrate further upstream during subsequent flow events forming conformable strata, or seismic resolution is insufficient to detect any discontinuity (e.g. Migeon *et al.*, 2000; Nakajima & Satoh, 2001; Pope *et al.*, 2018). Outcrop studies only occasionally mention evidence for long periods of inactivity between bedform reactivation (e.g. Lang *et al.*, 2017; Postma *et al.*, 2021). Possibly the start of deeper scouring, indicated in Figs 6 and 9 by 'R', represents the reactivation of cyclic-step activity. In the CB-units these scours can be identified at more or less regular intervals. Comparable truncations of cyclic-step deposits during reactivation have been documented from the Upper Eocene channel-levée complexes of the Brito Formation along the Pacific coast of Costa Rica and Nicaragua (Lang *et al.*, 2017) and from cyclic steps on modern delta slopes (Hage *et al.*, 2018; Vendettuoli *et al.*, 2019).

### Depositional model of the Cuatro Calas submarine volcanoclastic cyclic-step deposits

Based on the evidence presented, the sedimentary architecture of volcanoclastic cyclic-step

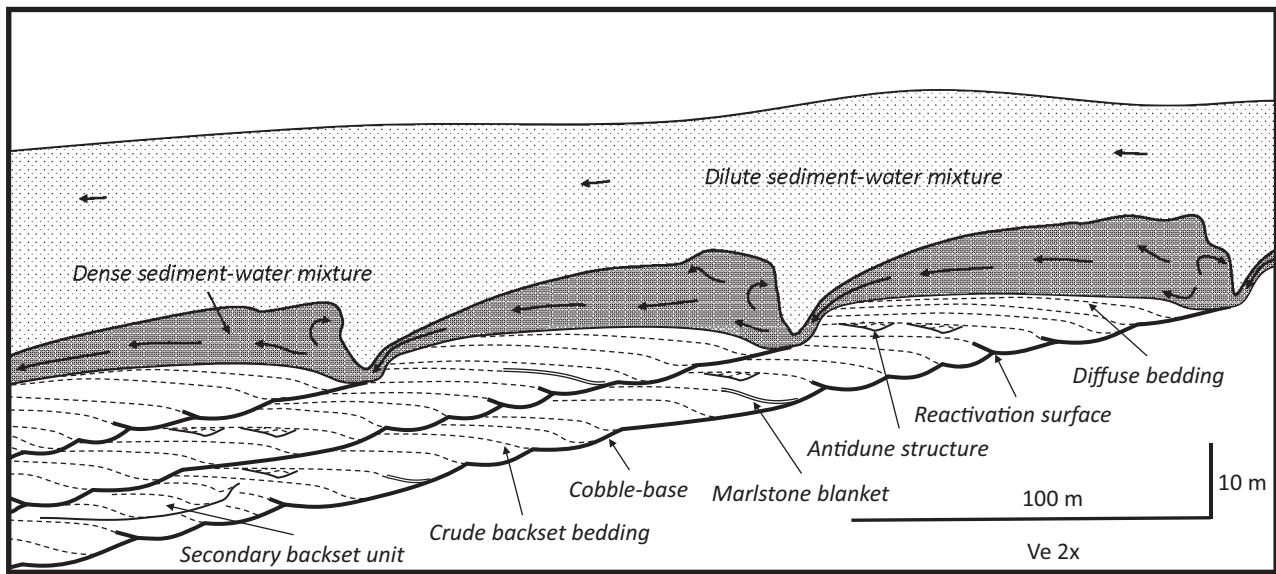


**Fig. 16.** Facies model of sandy and gravelly deposits of straight-crested cyclic steps generated during successive high-density flow events for conditions of palaeoslope,  $\beta = 2.5^\circ$ , bedform climbing angle,  $\alpha = 6^\circ$ , and cyclic step set height,  $S = 7$  m.

deposits in the sand-dominated lower part of the Cuatro Calas exposure is sketched in Fig. 16. A number of differences with the facies model described by Postma & Cartigny (2014) can be noticed (see also Figs 6 and 7): (i) the virtual absence of soft-sediment (flame) structures; (ii) the complication by secondary sigmoidal structures that lack a pervasive coarse-tail normal-graded lower interval; (iii) the presence of internal erosional surfaces in the lower part of the backset bedding; (iv) the absence of planar lamination ( $Tb_2$ ); and (v) the local absence of a structureless appearance of the graded basal division ( $Ta$ ).

The shape of bounding surfaces in the flow-parallel section shown in Fig. 16 is quite similar to the depositional signature of partially depositional crescentic cyclic steps of comparable size inferred from outcrops in late Quaternary glaciofluvial upper delta-slope sands, Québec (Ghienne *et al.*, 2020). However, in a flow-parallel section the unit bounding surfaces of the straight-crested cyclic steps of the Cuatro Calas case are more or less straight instead of the trough-shaped signature of the inferred crescentic bedforms in the Québécois case. In terms of bounding surface hierarchy introduced by Miall (1985) as adapted for application in turbidites by Postma *et al.* (2021) the set boundaries of CB-units can be classified as third-order surfaces. The reactivation surfaces in Fig. 16 may either

represent flow unsteadiness during a turbidite event or mark separate events. The boundaries of delimiting deposits of individual turbidite events, representing second-order surfaces, therefore can only be established with confidence if a reactivation surface is underlain by remnants of a marlstone blanket.

The model of Postma & Cartigny (2014) is mainly based on turbidites in confined conduits of the Miocene Buho submarine canyon, southeast Spain (Postma *et al.*, 2014). Hydraulic jumps in such channels could have been more powerful than those in unconfined settings, due to the steeper slope and more concentrated flow. More energetic hydraulic jumps could produce the strong lift forces required for flame structures which are rarely observed in the Cuatro Calas outcrop. Less energetic conditions could also result in less rapid erosion of the cyclic-step lee-side. This in turn would reduce aggradation rates directly downstream of the hydraulic jump to values insufficient for the accumulation of structureless sands.

A large proportion of the cyclic-step deposits of the Cuatro Calas outcrop consists of diffuse subhorizontal stratification. This proportion is likely even larger in many cases because seismic evidence often shows a climbing angle of the cyclic steps larger than the comparatively modest  $4^\circ$  to  $6^\circ$  applied in the facies model presented here (for an overview, see Slotman &

Cartigny, 2020). Therefore, the presence of thick layers of diffuse subhorizontal stratification is a strong criterion for the recognition of cyclic step deposits in outcrop and cores, especially when accompanied by coarse-tail normally graded intervals.

## CONCLUSIONS

A 67 m thick succession of up to 12 m thick cobble-based units is interpreted as the product of large cyclic steps accreting along a submarine volcanic slope. The depositional architecture is characterized by low-angle crude backsets passing upward into subhorizontal diffuse stratification. The cyclic-step units show an upward-thickening trend for the basal cobble-layers that eventually may encompass the whole sigmoidal structure. Sand-dominated cobble-based units show a 1 to 2 m thick pervasive coarse-tail normal grading at their base from cobbles with some boulders to coarse sand. The architecture of some of the cyclic-step units is complicated by the local occurrence of smaller, secondary sigmoidal structures lacking a basal gravelly division. These structures represent either the infill of cyclic-step troughs or were formed by antidunes or smaller cyclic steps superimposed on the stoss sides of the master bedforms. They are thought to have been formed by processes of adaptation of the cyclic-step bed morphology to density flows of lower strength. The cyclic-step height and length ranged between 65 to 460 m and 5 to 22 m, respectively. These values were calculated by a new method using measurements of sedimentary structures and an estimate of the subaqueous depositional slope. Two time-equivalent infill structures representing successive cyclic-step troughs indicate a bedform length of 170 m. The sigmoidal-shaped sand-dominated backsets are preserved in deposits with tabular geometries, that were produced by straight to sinuous crested cyclic steps, probably on an unconfined submarine slope. The lack of soft-sediment deformation structures and the local absence of a structureless lower division (Ta) may point to lower energy conditions as compared to cyclic steps in confined conduit channels described in previous literature. The straight-crested shape of the cyclic steps is possibly also an expression of less energetic conditions. The uppermost gravel-dominated cyclic-step units are interpreted to have formed by crescentic cyclic steps, reflecting accretion at a

shallower, more energetic proximal position with respect to the presumed coastal source of the density flows.

A generic feature confirmed by this study is that much of the stratification produced by sand-dominated cyclic steps on submarine slopes is diffuse subhorizontal stratification, whose thickness primarily depends on the climbing angle of the cyclic steps. Seismic evidence indicates that this inclination may be much more than the modest rate of 4° to 6° of the case discussed here, which may result in a much greater thickness of subhorizontal stratification than observed in the Cuatro Calas outcrop. However, diffuse subhorizontal stratification in itself may not be easily recognized as part of large sigmoidal backset structures formed by submarine cyclic steps unless exposed in large outcrops of excellent quality where its architectural relationship to sigmoidal-shaped structures can be proven.

## ACKNOWLEDGEMENTS

We thank the editorial team (A. Slootman, M. Cartigny, A. Normandeau, D. Ventra and S. Hubbard) for the opportunity to participate in this special issue. Daniele Casalbore, Giovanna Della Porta, Rebecca Englert, George Postma, Dario Ventra and an anonymous reviewer are gratefully acknowledged for their many helpful comments and constructive suggestions.

## DATA AVAILABILITY STATEMENT

The data that support the findings of this study are available from the corresponding author upon reasonable request.

## REFERENCES

- Alfaro, P., Delgado, J., Estévez, A., Soria, J.M. and Yébenes, A. (2002) Onshore and offshore compressional tectonics in the eastern Betic Cordillera (SE Spain). *Mar. Geol.*, **186**, 227–249.
- Allen, J.R.L. and Collinson, J.D. (1974) The superposition and classification of dunes formed by unidirectional aqueous flows. *Sed. Geol.*, **12**, 169–178.
- Allen, S.R., Hayward, B.W. and Mathews, E. (2007) A facies model for a submarine volcanoclastic apron: The Miocene Manukau Subgroup, New Zealand. *Bull. Geol. Soc. Am.*, **119**, 725–742.
- Aparicio, A. (2015) Características petrológicas y geoquímicas del nuevo afloramiento volcánico Mioceno de

- La Carolina (Águilas, Murcia, España). *Bol. R. Soc. Esp. Hist. Nat. Sec. Geol.*, **109**, 55–58.
- Arana-Castillo, R.** (2007) El patrimonio geológico de la región de Murcia. *Acad. Ciencias de la Región de Murcia*, 1–69. ISBN 84-611-3490-7.
- Bain, H.A. and Hubbard, S.M.** (2016) Stratigraphic evolution of a long-lived submarine channel system in the Late Cretaceous Nanaimo Group, British Columbia, Canada. *Sed. Geol.*, **227**, 112–122.
- Bardají, T.** (1999) Evolución Geomorfológica durante el Cuaternario de las Cuencas Neógenas litorales del Sur de Murcia y Norte de Almería. Thesis, Universidad Complutense de Madrid, 492 pp.
- Bellon, H., Bordet, P.Y. and Montenat, C.** (1982) Chronologie du magmatisme Néogène des Cordillères Bétiques (Espagne méridionale). *Bull. Soc. Géol. France*, **24**, 205–217.
- Best, J. and Fielding, C.R.** (2019) Describing fluvial systems: linking processes to deposits and stratigraphy. In: *River to Reservoir: Geoscience to Engineering* (Eds Corbett, P.W.M., Owen, A., Hartley, A.J., Pla-Pueyo, S., Barreto, D., Hackney, C. and Kape, S.J.). *Geol. Soc., London, Spec. Pubs*, **488**, 151–166.
- Boersma, J.R.** (1967) Remarkable types of mega cross-stratification in the fluvial sequence of a subrecent distributary of the Rhine. Amerongen; The Netherlands. *Geol Mijnbouw*, **46**, 217–225.
- Cartigny, M.J.B., Eggenhuisen, J.T., Hansen, E.W.M. and Postma, G.** (2012) Concentration-dependent flow stratification in experimental high-density turbidity currents and their relevance to turbidite facies models. *J. Sed. Res.*, **82**, 1047–1065.
- Cartigny, M.J.B., Postma, G., van den Berg, J.H. and Mastbergen, D.R.** (2011) A comparative study of sediment waves and cyclic steps based on geometries, internal structures and numerical modeling. *Mar. Geol.*, **280**, 40–56.
- Cartigny, M.J.B., Ventra, D., Postma, G. and Den Berg, J.H.** (2014) Morphodynamics and sedimentary structures of bedforms under supercritical-flow conditions: new insights from flume experiments. *Sedimentology*, **61**, 712–748.
- Cas, R.A.F. and Giordano, G.** (2014) Submarine volcanism: a review of the constraints, processes and products, and relevance to the Cabo de Gata volcanic succession. *Ital. J. Geosci.*, **122**, 262–277.
- Casalbore, D., Bosman, A., Martorelli, E. and Chiocci, F.L.** (2016a) Mass wasting features on the submarine flanks of Ventotene Volcanic Edifice (Tyrrhenian Sea, Italy). In: *Submarine Mass Movements and Their Consequences, Advances in Natural and Technological Hazards Research* (Ed. Lamarche, G.), pp. 285–292 Springer, New York.
- Casalbore, D., Bosman, A., Romagnoli, C. and Chiocci, F.L.** (2016b) Morphology of Salina offshore (southern Tyrrhenian sea). *J. Maps*, **12**, 725–720.
- Casalbore, D., Clare, M.A., Pope, E.L., Quartau, R., Bosman, A., Chiocci, F.L., Romagnoli, C. and Santos, R.** (2021) Bedforms on the submarine flanks of insular volcanoes: new insights gained from high resolution seafloor surveys. *Sedimentology*.
- Casalbore, D., Romagnoli, C., Bosman, A., Anzidei, M. and Chiocci, F.L.** (2018) Coastal hazard due to submarine canyons in active insular volcanoes: examples from Lipari Island (southern Tyrrhenian Sea). *J. Coast. Conserv.*, **22**, 989–999.
- Casalbore, D., Romagnoli, C., Bosman, A. and Chiocci, F.L.** (2014) Large-scale seafloor waveforms on the flanks of insular volcanoes (Aeolian Archipelago, Italy), with inferences about their origin. *Mar. Geol.*, **255**, 218–229.
- Chiocci, F.L., Romagnoli, C., Casalbore, D., Sposatoc, A., Martorelli, E., Alonso, B., Casase, D., Conte, A.M., Di Bella, L., Ercillad, G., Estradad, F., Falesea, F., Farrand, M., Forleoa, V., Frezza, V., Hipolitog, A., Lebania, A., Maistoa, F., Pachecog, J., Pimentelg, A., Quartauh, R., Roqueh, I., Sampaioi, C., Santoroa, P.C. and Temperai, F.** (2012) Bathymorphological setting of Terceira island (Azores) after the FAIVI cruise. *J. Maps*, **9**, 590–595.
- Clare, M.A., Le Bas, T., Price, D.M., Hunt, J.E., Sear, D., Cartigny, M.J.B., Vellinga, A., Symons, W., Firth, C. and Cronin, S.** (2018) Complex and cascading triggering of submarine landslides and turbidity currents at volcanic islands revealed from integration of high-resolution onshore and offshore surveys. *Front. Earth Sci.*, **6**, 24.
- Clement, C.P., Pacheco-Martinez, H.A., Swift, M.R. and King, P.J.** (2010) The water-enhanced Brazil nut effect. *Europhys. Lett.*, **91**, 54001.
- Coppier, G., Griveaud, P., Larouziere, F.D., Montenat, C.H. and Ott d'Estevou, P.H.** (1989) Example of Neogene tectonic indentation in the Eastern Betic Cordilleras: the Arc of Águilas (Southeastern Spain). *Geodin Acta*, **2**, 27–51.
- Cornard, P.H. and Pickering, K.T.** (2019) Supercritical-flow deposits and their distribution in a submarine channel system, Middle Eocene, Ainsa basin, Spanish Pyrenees. *J. Sed. Res.*, **89**, 576–597.
- Dabrio, C., Bardají, T., Zazo, C. and Goy, J.** (1991) Effects of sea-level changes on a wave-worked Gilbert-type delta (Late Pliocene, Águilas Basin, SE Spain). *Cuadernos Geol. Ibérica*, **15**, 102–127.
- Dietrich, P., Ghienne, J.F., Normandeau, A. and Lajeunesse, P.** (2016) Upslope-migrating bedforms In a proglacial sandur delta: cyclic steps from river-derived underflows? *J. Sediment. Res.*, **86**, 112–122.
- Do Couto, D., Gorini, C., Jolivet, L., Lebret, N., Augier, R., Gumiaux, C., d'Acremont, E., Ammar, A., Jabour, H. and Auxietre, J.-L.** (2016) Tectonic and stratigraphic evolution of the Western Alboran Sea Basin in the last 25 Myrs. *Tectonophysics*, **677–678**, 280–211.
- Dzulynski, S. and Sanders, J.E.** (1962) Current marks on firm mud bottoms. *Trans. Connecticut Acad. Arts Sci.*, **42**, 57–96.
- Englert, R.G., Hubbard, S.M., Cartigny, M.J.B., Clare, M.A., Counts, D.S., Hage, S., Hughes Clarke, J., Jobe, Z., Lintern, D.G., Stacey, C. and Ventettuoli, D.** (2021) Quantifying the three-dimensional stratigraphic expression of cyclic steps by integrating seafloor and deep-water outcrop observations. *Sedimentology*.
- Fedele, J.J., Hoyal, D.C., Barnaal, Z., Tulenko, J. and Awalt, S.** (2016) Bedforms Created by gravity flows. In: *Autogenic Dynamics in Sedimentary Systems* (Eds Budd, D., Hajek, E. and Purkis, S.), *SEPM Spec. Publ.*, **106**, 95–121, Tulsa.
- Fielding, C.R.** (2006) Upper flow regime sheets, lenses and scour fills: extending the range of architectural elements for fluvial sediment bodies. *Sed. Geol.*, **190**, 227–240.
- Ghienne, J.-F., Normandeau, A., Dietrich, P., Bouysson, M., Lajeunesse, P. and Schuster, M.** (2020) The depositional signature of cyclic steps: a late Quaternary analogue compared to modern active delta slopes. *Sedimentology*.
- Griveaud, P., Coppier, G., Montenat, C. and Ott d'Estevou, P.** (1990) Le Néogène des Sierras D'Águilas. In: *Les bassins Néogènes du domaine Bétique oriental (Espagne): Tectonique et sédimentation dans un couloir de*



- décrochement. Première partie: Etude régionale (Ed. Montenat, C.), *Doc et Trav. Inst. Geol. Albert-de-Lapparent*, **12-12**, 221–228.
- Hage, S., Cartigny, M.J.B., Clare, M.A., Sumner, E.J., Vendettuoli, D., Hughes Clarke, J.E., Hubbard, S.M., Talling, P.J., Gwyn Lintern, D., Englert, R.G., Vardy, M.E., Hunt, J.E., Yokokawa, M., Parsons, D.R., Hizzett, J.L., Azpiroz-Zabala, M. and Vellinga, A.J. (2018) How to recognize crescentic bedforms formed by supercritical turbidity currents in the geologic record: insights from active submarine channels. *Geology*, **46**, 562–566.
- Harvey, A.M. (2002) Effective timescales of coupling within fluvial systems. *Geomorphology*, **44**, 175–201.
- Heinrichs, T. (1984) The Umsoli chert, turbidite testament for a major phreatoplinian event at the onverwacht/fig tree transition (Swaziland supergroup, Archaean, South Africa). *Precamb. Res.*, **24**, 227–282.
- Hiscott, R.N. (1994) Traction-carpet stratification in turbidites—fact or fiction? *J. Sed. Res.*, **A64**, 204–208.
- Hiscott, R.N. and Middleton, G.V. (1979) Depositional mechanics of thick-bedded sandstones at the base of a submarine slope, Tourrelle Formation (Lower Ordovician), Québec, Canada. In: *Geology of Continental Slopes* (Eds Doyle, L.J. and Pilkey, O.H.), *SEPM Spec. Publ.*, **27**, 207–226.
- Hughes Clarke, J.E. (2016) First wide-angle view of channelized turbidity currents links migrating cyclic steps to flow characteristics. *Nat. Commun.*, **7**, 11896.
- Ito, M. (2010) Are coarse-grained sediment waves formed as downstream-migrating antidunes? Insight from an early Pleistocene submarine canyon on the Boso Peninsula. *Jpn. Sed. Geol.*, **226**, 1–8.
- Kennedy, J.F. (1961) *Stationary Waves and Antidunes in Alluvial Channels*. Rep. K11-R-2, W.M. Keck Laboratory of Hydraulics and Water Resources, California Institute of Technology, Pasadena, CA. 146 pp.
- Kleinbans, M.G. (2004) Sorting in grain flows at the lee side of dunes. *Earth Sci. Rev.*, **65**, 75–102.
- Kostic, S. (2011) Modeling of submarine cyclic steps: controls on their formation, migration, and architecture. *Geosphere*, **7**, 294–204.
- Kostic, S. (2014) Upper flow regime bedforms on levees and continental slopes: turbidity current flow dynamics in response to fine-grained sediment waves. *Geosphere*, **10**, 1094–1102.
- Lang, J., Brandes, C. and Winsemann, J. (2017) Erosion and deposition by supercritical density flows during channel avulsion and backfilling: Field examples from coarse-grained deepwater channel-levée complexes (Sandino Forearc Basin, southern Central America). *Sed. Geol.*, **249**, 79–102.
- Lang, J. and Winsemann, J. (2012) Lateral and vertical facies relationships of bedforms deposited by aggrading supercritical flows: From cyclic steps to humpback dunes. *Sed. Geol.*, **296**, 26–54.
- Liao, C.-C. and Hsiau, S.-S. (2016) Transport and segregation phenomena in vibrating granular beds. *KONA Powder Part. J.*, **22**, 109–126.
- Lowe, D.R. (1975) Water escape structures in coarse-grained sediments. *Sedimentology*, **22**, 157–204.
- Lowe, D.R. and LoPiccolo, R.D. (1974) The characteristics and origins of dish and pillar structures. *J. Sed. Petr.*, **44**, 484–501.
- Martinius, A.W. and Van den Berg, J.H. (2011) *Atlas of Sedimentary Structures in Estuarine and Tidally-Influenced River Deposits of the Rhine-Meuse-Scheldt System: Their Application to the Interpretation of Analogous Outcrop and Subsurface Depositional Systems*. pp. 298 EAGE Publications, Houten. ISBN 978-90-73834-11-8.
- Martinius, A.W., Jablonski, B.V.J., Fustic, M., Strobl, R. and Van den Berg, J.H. (2015) Fluvial to tidal transition zone facies in the McMurray Formation (Christina River, Alberta, Canada), with emphasis on the reflection of flow intensity in bottomset architecture. In: *Fluvial-tidal Sedimentology* (Eds Ashworth, P.J., Best, J.L. and Parsons, D.R.), *Dev. Sedimentology*, **68**, 448–480.
- Mastbergen, D.R. and Van den Berg, J.H. (2002) Breaching in fine sands and the generation of sustained turbidity currents in submarine canyons. *Sedimentology*, **50**, 625–627.
- Massari, F. (2017) Supercritical-flow structures (backset-bedded sets and sediment waves) on high-gradient clinoform systems influenced by shallow-marine hydrodynamics. *Sed. Geol.*, **260**, 72–95.
- Miall, A.D. (1985) Architectural-element analysis: a new method of facies analysis applied to fluvial deposits. *Earth-Sci. Rev.*, **22**, 261–208.
- Middleton, G.V. (1965) Antidune cross-bedding in a large flume. *J. Sed. Petrol.*, **25**, 922–927.
- Migeon, S., Savoye, B. and Faugeres, J.C. (2000) Quaternary development of migrating sediment waves in the Var deep-sea fan: distribution, growth pattern, and implication for levee evolution. *Sed. Geol.*, **122**, 265–292.
- Mills, C. (1982) Genesis and diagnostic value of soft-sediment deformation structures, a review. *Sed. Geol.*, **25**, 82–104.
- Mulder, T. (2011) Gravity processes and deposits on continental slope, rise and abyssal plains. In: *Deep-Sea Sediments. Development in Sedimentology*, **62** (Eds Hüneke, H. and Mulder, T.). Elsevier, Amsterdam, pp. 25–148.
- Nakajima, T. and Satoh, Y. (2001) The formation of large mudwaves by turbidity currents on the levees of the Toyama deep-sea channel, Japan Sea. *Sedimentology*, **48**, 425–462.
- Ono, K. and Plink-Björklund, P. (2018) Froude supercritical flow bedforms in deepwater slope channels? Field examples in conglomerates, sandstones and fine-grained deposits. *Sedimentology*, **65**, 629–669.
- Ono, K., Plink-Björklund, P., Eggenhuisen, J.P. and Cartigny, M.J.B. (2021) Froude supercritical flow processes and sedimentary structures: new insights from experiments with a wide range of grain sizes. *Sedimentology*.
- Paul, C.K., Talling, P.J., Maier, K.L., Parsons, D., Xu, J., Caress, D.W., Gwiazda, R., Lundsten, E.M., Anderson, K., Barry, J.P., Chaffey, M., Chaffey, M., O'Reilly, T., Rosenberger, K.J., Gales, J.A., Kieft, B., Mary McGann, M., Simmons, S.M., McCann, M., Sumner, M., Clare, M.A. and Cartigny, M.J. (2018) Powerful turbidity currents driven by dense basal layers. *Nat. Commun.*, **9**, 4114.
- Ponce, J.J. and Carmona, N. (2011) Coarse-grained sediment waves in hyperpycnal clinoform systems, Miocene of the Austral foreland basin, Argentina. *Bull. Geol. Society Am.*, **29**, 762–766.
- Pope, E.L., Jutzeler, M., Cartigny, M.J.B., Shreeve, J., Talling, P.J., Wright, I.C. and Wysoczanski, R.J. (2018) Origin of spectacular fields of submarine sediment waves around volcanic islands. *Earth Planet. Sci. Lett.*, **492**, 12–24.
- Postma, G. (1982) Water escape structures in the context of a depositional model of a mass flow conglomeratic fan-delta

- (Abrija Formation, Pliocene, Almeria Basin, SE Spain). *Sedimentology*, **20**, 91–102.
- Postma, G. and Cartigny, M.J.B.** (2014) Supercritical and subcritical turbidity currents and their deposits—a synthesis. *Geology*, **42**, 987–990.
- Postma, G., Cartigny, M. and Kleverlaan, K.** (2009) Structureless, coarse-tail graded Bouma Ta formed by internal hydraulic jump of the turbidity current? *Sed. Geol.*, **219**, 1–6.
- Postma, G. and Kleverlaan, K.** (2018) Supercritical flows and their control on the architecture and facies of small-radius sandrich fan lobes. *Sed. Geol.*, **264**, 52–70.
- Postma, G., Kleverlaan, K. and Cartigny, M.J.B.** (2014) Recognition of cyclic steps in sandy and gravelly turbidite sequences and consequences for the Bouma facies model. *Sedimentology*, **61**, 2268–2290.
- Postma, G., Hoyal, D.C., Abreu, V., Cartigny, M.J.B., Demko, T., Fedele, J.J., Kleverlaan, K. and Pederson, K.H.** (2016) Morphodynamics of supercritical turbidity currents in the channel-lobe transition zone. In *Submarine Mass Movements and their Consequences* (Eds Postma, G. et al.). *Advances in Natural and Technological Hazards Research*, **41**, 461–478.
- Postma, G., Lang, J., Hoyal, D.C., Fedele, J.J., Demko, T., Abreu, V. and Pederson, K.H.** (2021) Reconstruction of bedform dynamics controlled by supercritical flow in the channel-lobe transition zone of a deep-water delta (Sant Llorenç del Munt, NE Spain, Eocene). *Sedimentology*.
- Romagnoli, C., Casalbone, D. and Chiocci, F.L.** (2012) La Fossa Caldera breaching and submarine erosion (Vulcano island, Italy). *Mar. Geol.*, **202–206**, 87–98.
- Santos, R., Quartau, R., da Silveira, A.B., Ramalho, R. and Rodrigues, A.** (2019) Gravitational, erosional, sedimentary and volcanic processes on the submarine environment of Selvagens Islands (Madeira Archipelago, Portugal). *Mar. Geol.*, **415**, 105945.
- Schumm, S.A., Bean, D.W. and Harvey, M.D.** (1982) Bedform-dependent pulsating flow in medano creek, southern colorado. *Earth Surf. Process. Landforms*, **7**, 17–28.
- Silva, P.G., Goy, J.L., Somoza, L., Zazo, C. and Bardají, T.** (1992) Landscape response to strike-slip faulting linked to collisional settings: quaternary tectonics and basin formation in the Eastern Betics, southeastern Spain. *Tectonophysics*, **224**, 289–202.
- Symons, W.O., Sumner, E.J., Talling, P.J., Cartigny, M.J.B. and Clare, M.A.** (2016) Large-scale sediment waves and scours on the modern seafloor and their implications for the prevalence of supercritical flows. *Mar. Geol.*, **271**, 120–148.
- Slootman, A., De Boer, P.L., Cartigny, M.J., Samankassou, E. and Moscariello, A.** (2019) Evolution of a carbonate delta generated by gateway-funnelling of episodic currents. *Sedimentology*, **66**, 1202–1240.
- Slootman, A. and Cartigny, M.J.B.** (2020) Cyclic steps: review and aggradation-based classification. *Earth Sci. Rev.*, **201**, 102949.
- Slootman, A., Vellinga, A.J. and Cartigny, M.J.B.** (2021) The depositional signature of high-aggradation chute-and-pool bedforms: the build-up-and-fill structure. *Sedimentology*.
- Sohn, Y.K.** (1997) On traction-carpet sedimentation. *J. Sed. Res.*, **67**, 502–509.
- Sohn, Y.K., Rhee, C.W. and Kim, B.C.** (1999) Debris flow and hyperconcentrated flood-flow deposits in an alluvial fan, northwestern part of the cretaceous yongdong basin, central Korea. *J. Geol.*, **107**, 111–122.
- Southard, J.B. and Boguchwal, A.L.** (1990) Bed configurations in steady unidirectional water flows. Part 2. Synthesis of flume data. *J. Sed. Petrol.*, **60**, 658–679.
- Sumner, E.J., Lawrence, A., Amy, L.A. and Talling, P.J.** (2008) Deposit structure and processes of sand deposition from decelerating sediment suspensions. *J. Sed. Res.*, **78**, 529–547.
- Sumner, E.J., Talling, P.J., Amy, L.A., Wynn, R.B., Stevenson, C. and Frenz, M.** (2012) Facies architecture of individual basin-plain turbidites: comparison to existing models and implications for flow processes. *Sedimentology*, **59**, 1850–1887.
- Talling, P.J., Masson, D.G., Sumner, E.J. and Malgesini, G.** (2012) Subaqueous sediment density flows: depositional processes and deposit types. *Sedimentology*, **59**, 1927–2002.
- Van den Berg, J.H., Martinus, A.W. and Houthuys, R.** (2017) Breaching-related turbidites in fluvial and estuarine channels: Examples from outcrop and core and implications to reservoir models. *Mar. Petrol. Geol.*, **82**, 178–205.
- Vendettuoli, D., Clare, M.A., Clarke, J.H., Vellinga, A., Hizzet, J., Hage, S., Cartigny, M.J.B., Talling, P.J., Waltham, D., Hubbard, S.M., Stacey, C. and Lintern, D.G.** (2019) Daily bathymetric surveys document how stratigraphy is built and its extreme incompleteness in submarine channels. *Earth Planet. Sci. Lett.*, **515**, 221–247.
- Ventra, D., Cartigny, M.J.B., Bijkerk, J.F. and Acikalin, S.** (2015) Supercritical-flow structures on a Late Carboniferous delta front: Sedimentologic and paleoclimatic significance. *Geology*, **42**, 721–724.
- White, J.D.L.** (1996) Pre-emergent construction of a lacustrine basaltic volcano, Pahvant Butte, Utah (USA). *Bull. Volcanol.*, **58**, 249–262.
- Winsemann, J. and Seyfried, H.** (1991) Response of deep-water fore-arc systems to sea-level changes, tectonic activity and volcanoclastic input in Central America. In: *Sedimentation, Tectonics and Eustasy: Sea-Level Changes at Active Margins* (Ed. Macdonald, D.I.M.). *IAS Spec. Publ.*, **12**, 272–292.
- Zazo, C., Goy, J.L., Dabrio, C.J., Lario, J., González-Delgado, J.A., Bardají, T., Hillaire-Marcel, C., Cabero, A., Ghaleb, B., Borja, F., Silva, P.G., Roquero, E. and Soler, V.** (2012) Retracing the Quaternary history of sea-level changes in the Spanish Mediterranean-Atlantic coasts: geomorphological and sedimentological approach. *Geomorphology*, **196**, 26–49.
- Zhong, G., Cartigny, M.J., Kuang, Z. and Wang, L.** (2015) Cyclic steps along the South Taiwan Shoal and West Penghu submarine canyons on the northeastern continental slope of the South China Sea. *Geol. Soc. Am. Bull.*, **127**, 804–824.

Manuscript received 22 March 2020; revision accepted 19 November 2020

## Supporting Information

Additional information may be found in the online version of this article:

**Data S1.** Photographic pictures of the western part of the cliff outcrop.